SISSA - SCUOLA
INTERNAZIONALE
SUPERIORE
DI STUDI AVANZATI
TRIESTE
Strada Costiera 11

ISAS - INTERNATIONAL SCHOOL FOR ADVANCED STUDIES

Dynamical processes on fractals: fractal dynamics of proteins probed by electronic and nuclear relaxation and numerical results on fractal surfaces.

Thesis submitted for the Degree:

Magister Philosophiae

Candidate

Dr. Gilberto Giugliarelli

Supervisor

Prof. Attilio Stella

Academic Year 1987/88

TRIESTE

Contents

Introduction

The study of the static and dynamic properties of complex and disordered systems constitutes one of the challenges of modern physics. Often, complexity and disorder are associated to scaling symmetry and fractality. Indeed, fractality is a characterizing property of a large class of systems in physics.

Hystorically, it is worth noticing, that the development of fractal theory was strongly stimulated by low temperature relaxation experiments in proteins.[1] The interpretation of these measurements with a dynamical fractal model (see chapter 4 for more details) has marked an important step in the development of our understanding of fractals.

To some extent, dealing with fractals amount to approach problems in critical phenomena. Such phenomena occur in many fields, far beyond the traditional one of phase transitions (e.g. in solid state physics, biology, astrophysics, etc...). The emphasis on fractals reflects the present attitude to understand critical phenomena more deeply from a geometrical point of view. On the other hand, the tools of critical phenomena theory, e.g., the renormalization group, are widely used to study fractal properties.

As stated above, fractal structures often occur in nature.Typical examples are polymers in solution, aggregates in irreversible growth processes, percolation clusters, etc... All these examples refer to structures which posses a sort of hierarchical

organization in their spatial conformation. There are, however, other more general examples of "fractality" relevant to physics, in which the hierarchical organization does not refer to geometry, but, e.g., to time or energy scales in a problem. These kind of hierarchies are expect to be a key for the explanation of many puzzles, e.g., in condensed matter physics (e.g. glasses)[2,3] or in the dynamics of proteins (protein quakes).[4]

Our primary interest is the study of structural and dynamical properties of proteins by electronic and nuclear resonance techniques. In view of the possible relevance of fractal ideas in the interpretation of the experimental facts, we also felt the necessity of developing in parallel a study of fractal dynamics from a more theoretical and general point of view. In some sense, this choice somehow follows the hystorical path by which theoretical fractal ideas first developed in the early eighties.

This thesis presents both experimental and theoretical results. The latter are not always very directly related to experimental results, because the complexity of the systems studied and the effects to take into account prevents the possibility of developing very realistic and quantitative models. In view of this, we rather tried to understand general qualitative features of fractal dynamics, which can be of relevance to protein experiments, as to other biophysical problems more indirectly. On the other hand, these problems have their own justification in a more theoretical context. As shown in this thesis the study of models of fractal dynamics can provide clues to the understanding of issues also in related fields, like polymer or membrane statistics.

So that, after having summarized in the first three chapters the structural and dynamical properties of fractals and proteins respectively, in the last two we present the experimental and theoretical results above mentioned.

In chapter 4, a review of the Stapleton's experimental results on protein relaxation and a new set of data for copper-protein Plastocyanin are presented togheter with an

original theoretical model able to interprete, by using the main concepts of fractal dynamics, the water nuclear relaxation in the presence of biomolecules.

Finally, in chapter 5 the results of the calculations of the diffusion exponents of random walks on a fractal surface are reported.

References

1. H.J.Stapleton, J.P.Allen, C.P.Flynn, D.G.Stinson andS.R.Kurtz, Phys. Rev. Lett., **45**,1456(1980)
2. M.Mezard, G.Parisi, N.Sourlas, & M.Virasoro, *Phys.Rev.Lett.*, **52**, 1156(1894)
3. R.G.Palmer, D.L.Stein, E.Abrahams & P.W.Anderson, *Phys.Rev.Lett.*, **53**, 958(1984)
4. A.Ansari, J.Berendsen, S.F.Bowne, H.Frauenfelder, I.E.T.Iben, T.B.Sauke, E.Shyamsunder & R.D.Young, *Proc.Natl.Acad.Sci. USA*, **82**, 5000(1985)

Chapter 1

Geometrical features of fractal structures

This chapter is devoted to give an introduction about the main concepts and quantities of the geometry of fractal structures.

1.1 Self-similarity

Fractal concepts were developed originally by mathematicians about a century ago, under the influence of a crisis in mathematics. The divulgation of among physicists of these geometrical ideas, and even the term "fractals" is due to B.Mandelbrot.[1] To introduce the ideas of fractals we will sketch some examples (taken from physics of critical phenomena or other fields) which will bring the reader to experience directly the properties of these systems.

Lets think, e.g., to a fluid near its critical point. In the gas phase, due to strong fluctuations, there will be droplets of liquid phase. At the critical point the characteristic size of the droplets will become large and large. A clear picture of this phenomenon is given in this way: each droplet is itself critical and then contain small vapour droplets which again contain small liquid droplets, etc.... The system

do not show a characteristic length scale in the sense that we can find droplets with all possible sizes

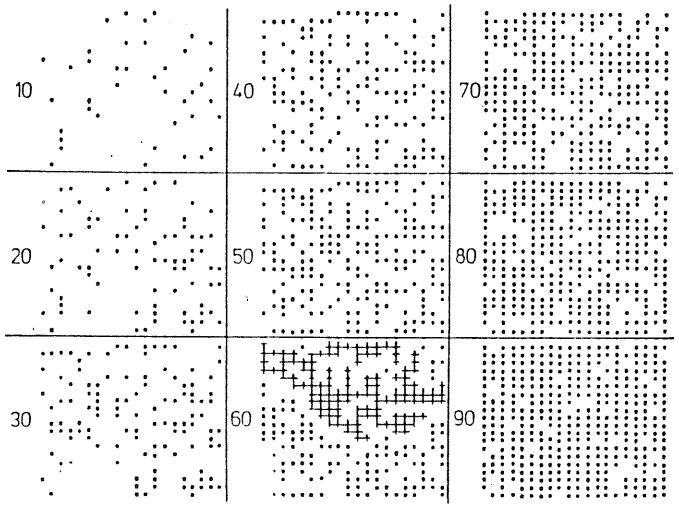

Fig. 1.1. Examples of percolation on a 20x20 squared lattice, for p = 0.1, 0.2, ... , 0.9. Occupied sites are shown as dots, empty sites are not shown. The overlapping crosses at 60 percent probability give the largest "percolating" cluster.

and then each part of the system can be seen as statistically similar to a scaled larger part of the whole system.

Another example of the statistical self-similarity at criticality is provided by the infinite percolation cluster at threshold[2] (for examples on percolation see Fig. 1.1). If we compare two equal-sized parts from two reductions with a different scale factor of such clusters (supposing the reduction is such that the lattice spacing is no longer resolvable), we cannot recognize which one involves the largest reduction factor, because the two are statistically similar. This means that the original pattern has self-similar appearences: on all scales it contains parts that looks like the whole object.

Self-similarity constitutes a peculiar property of the fractal objects. The main ideas here reported by the examples give a clear of the meaning of self-similarity.

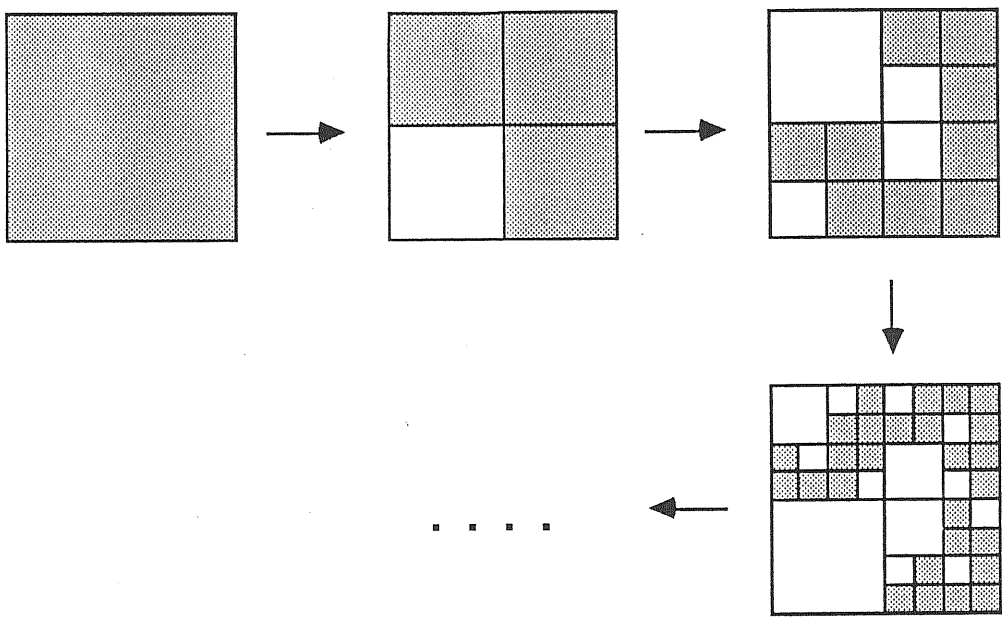

Fig. 1.2. Geometrical fractal

1.2 Fractal dimensionality

To introduce the concepts of fractal dimension let us consider the following construction. Take a square; divide it in four equal parts; choose one of these at random and leave it empty; repeate this procedure with the three remaning parts; etc... (see Fig. 1.2) In this costruction, if iterated long enough, one can see a high degree of self-similarity in the structure obtained (by the way, this is very similar to an infinite percolation cluster). An important feature that characterizes such geometrical fractal structure is the capacity dimension, commonly called "fractal dimension",[1] which describes how the number of points of the structure or the mass M grows with the linear size R:

$$M \sim R^{d} \qquad (1.1)$$

This is a generalization of the relation for compact objects with uniform density in d dimensions ($M \sim R^d$). One can construct even more simple self-similar structures, in which randomness does not enter. Since in our construction one quarter of the square contains one third of its material, we easely find $\bar{d} = \log 3 / \log 2 \approx 1.5849$. Another well known fractal

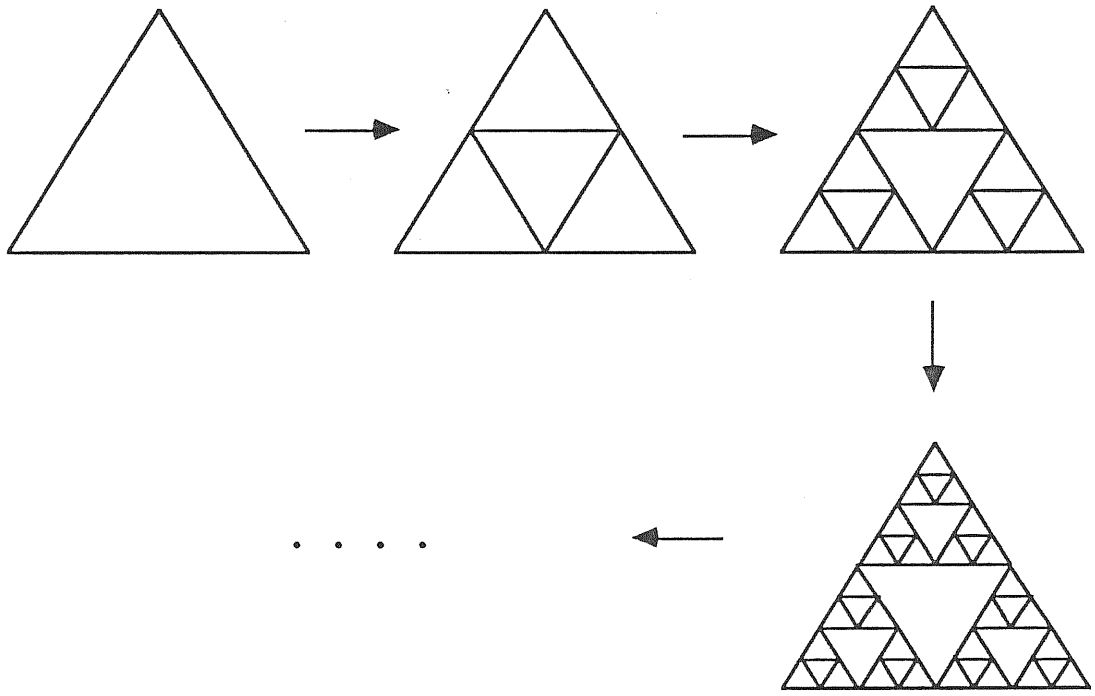

Fig. 1.3. Sierpinski gasket

(deterministic fractal) is the Sierpinski gasket reported in Fig. 1.3. Its fractal dimension is $\bar{d} = \log 3 / \log 2 \approx 1.5849$ as can be easely evaluated. To conclude this review of deterministic fractals we show in Fig. 1.4 the triangular Koch curve ($\bar{d} = \log 4 / \log 3 \approx 1.2618$).

One of the consequences of the self-similarity property and the non-integer value of $\bar{d}$ and that $\bar{d} < d$ (d is alwais smaller than the dimension of the embedding space),

is that the density of a fractal depends on its size R, and decreases to zero as the size R diverges. We have obviously

$$\rho \sim R^{\bar{d}-d} \tag{1.2}$$

This property is quite remarkable and important in understading the nature of the fractal objects.

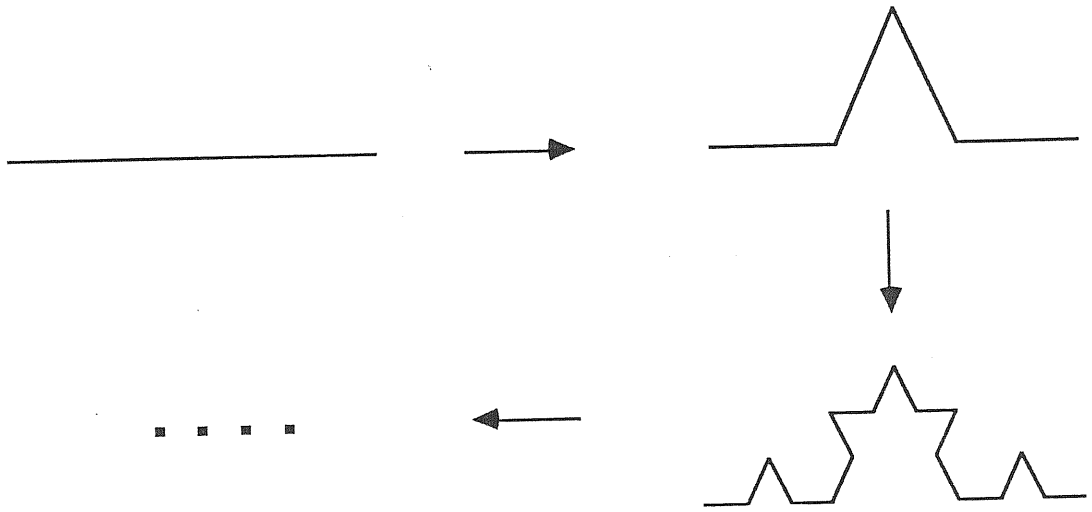

Fig. 1.4. Triadic Koch curve

1.3 Random fractals

In general we should make a distinction between the fractals we can construct by following some geometrical law and the fractals we find in nature. Usually, real structures exhibite fractal properties only on a statistical base. This means that a definition of a fractal dimension in a real case is possible only by considering some kind of ensemble averages. Remarkable examples are the incipient infinite percolation cluster above mentioned, the droplets of the Ising model, the random walk or the linear

polymers. For a random walk (RW) of N steps in d-dimensional space, the average end-to-end distance is given by

$$<R> \sim N^{1/2} \equiv N^{1/d_w} \qquad (1.3)$$

with $d_W = 2$ when $d \geq 2$. d_W can be taken as equal 2 also in a one-dimensional space.

Another example of random fractal model, which reproduces very well the conformational properties of real linear polymers in "good" solvents, is the so called self avoiding walk (SAW). One finds

$$<R> \sim N^{\nu} \equiv N^{1/d_{SAW}} \qquad (1.4)$$

where in this case $d_{SAW} < 2$, for $d < 4$. In a two-dimensional space d_{SAW} is found to be equal 4/3,[3] while in three dimensions the existing montecarlo simulations[4] predicted a value of d_{SAW} close to 5/3. The law (1.4) tells us that, in a statistical sence, the dominant configuration of a SAW share some of the features of a Koch curve (at least in two dimensions).

To conclude this chapter we would like to sketch the main concepts of a simple theoretical approach to the fractal dymension of polymers due to Flory.[5] In spite of the fact that it constitutes only an approximated method, it turns out to be extremely powerfull in predicting the exponents of RW and SAW. Such method is also in use for more complicated fractals, like surfaces, as we will see in chap. 5. Let us then consider a linear polymer in the solvent. Flory expects that R (end to end distance) is determined by two competing effects: on the one hand monomer-monomer repulsion tend to swell the coil and to increase R. On the other side entropy tends to disfavour big values of R, because, the larger R is, the fewer configurations can be found compatible with it. The idea is then to parametrize the free energy, which, in a mean field way, can be estimated as being proportional to the average density of monomers times N, i.e. $U \sim N^2/R^d$. The entropy can be guessed from the result for a Gaussian chain (RW), in which the probability of elongation R is proportional to $\exp(-cR^2/N)$, or $-TS \sim R^2/N$. Thus

$$F = U - TS \approx a \frac{N^2}{R^d} + b \frac{R^2}{N} \qquad (1.5)$$

By extremalization of this relation we get

$$R \sim N^{3/(2+d)} \qquad (1.6)$$

As can be easily seen this formula reproduces the above mentioned results for SAW exponents.

References

1. B.B.Mandelbrot, *"Fractals, Forms, Chance and Dimensions"*, Freeman, San Francisco (1979) & *"The Fractal Geometry of Nature"*, Freeman, San Francisco (1982)
2. D.Stauffer, *Phys.Rep.*, **54**, 1 (1979)
3. B.Nienhuis, *Phys.Rev.Lett.*, **49**, 1063(1982)
4. P.G.deGennes, *"Scaling Concepts on Polymer Physics"*, Cornell University Press, Ithaca (1979)
5. P.J.Flory, *"Principles of Polymer Chemistry"*, Cornell University Press, (Ithaca, 1969)

Chapter 2

Dynamics of fractal structures

Once characterized the geometrical and conformational properties of fractal systems we start in this chapter to approach their dynamical properties. In particular, we shall be interested on the low frequency behaviour of the density of vibrational states since most of the anomalous dynamical features displayed by fractal structures are related to this quantity.

2.1 The general problem

The fractal structures found in nature are not only interesting because of their self-similar geometry, but also because they can be the context in which, e.g., dynamical processes occur. These processes can be of very different kind: diffusion, spin waves, harmonic vibration, etc...

The first dynamical problem on a fractal structure was proposed by de Gennes in 1976 (the ant in the labyrinth).[1] More recently problems of this kind were considered also in connection with the ambitious program of understanding anomalous relaxation properties of biopolymers by Stapleton and co-workers and by Alexander and

Orbach.[2,3] These authors also introduced the key concept of spectral dimension as the dimension describing the scaling of the density of vibrational eigenstates of fractal structures.

Working in the elastic approximation, so that the system can be thought as an ensamble of particles connected each other by springs (usually with the first neighbors, but the considerations we will report in this section are generally valid), the equation of motion can be written simply as

$$m_i \ddot{u}_i = \sum_{<j>} K_{ij} (u_j - u_i) \qquad (2.1)$$

where m_i and u_i are the mass and the displacement vector of the i-th particle; K_{ij} is the matrix of the elastic costants of the connected particles. The sum is made over the particles connected to the ith .

In writing eq. (2.1) we have used a simplified scalar model.[4] In general for three-dimensional system the equation of motion can have a more complicated form[5] since the possible presence of directional forces and the impossibility of separate the motion in particular directions as it is always possible to do for two-dimensional system (at least for the transverse phonons). The limitations of eq. (2.1), however, does not decrease the general validity of the considerations we wont to discuss in the resting part of this section.

The solution of this set of differential equations is obtained by considering periodic functions as $u_i(t) = u_i^{(0)} e^{i\omega t}$. Moreover by considering the matrix **H** defined as follow

$$H_{ij} = - \frac{K_{ij}}{\sqrt{m_i m_j}} \quad \text{when } i \neq j; \quad H_{ii} = \frac{1}{m_i} \sum_{<j>} K_{ij} \qquad (2.2)$$

and $u_i' = \frac{u_i}{\sqrt{m_i}}$ the eq. (2.1) can be rewritten (after substituted the u's with the new functions) in the form

$$\mathbf{H}\ \mathbf{u}' = \omega^2\ \mathbf{u}' \tag{2.3}$$

The matrix **H** is a simmetric matrix and the **u'** constitutes now the vector of the displacement amplitudes for each particle of the system. The eigenvalues equation (2.3) is solved by diagonalizing the matrix **H**. Its eigenvalues (ω^2) are the squared eigen frequencies of the system while the eigen vectors are correspond to the motion amplitude of each particle for the specific mode.In this approximation the motion of the system in then represented by a linear combination of all the harmonic modes.

When the number of particles becomes large, the solution of eq. (2.3) becomes quite hard because of the memory and time consumption. In any case if the frequencies of the systems have been achieved the spectrum of frequencies (density of vibrational states) is usually obtained by making an histogram of the frequencies.

2.2 Diffusion and harmonic vibration problem

An alternative way to obtain the frequency spectrum of the harmonic modes for a particle system that is particularly usefull for fractal systems, can be developed by using the connection existing between the solution of harmonic problem and the diffusional problem. It is instructive to follow directly the development of the method.

A diffusion problem is formally posed by the following system of equations

$$\frac{dP_i}{dt} = \sum_{<j>} W_{ij}\ (P_j - P_i) \tag{2.4}$$

where now P_i are the probabilities of finding the diffusing particle in the ith site and the W_{ij} is the rate of jumping between the sites i and j. By following a strategy similar to that we have seen above, we define now

$$H_{ij} = -W_{ij} \text{ when } i \neq j; \qquad H_{ii} = \sum_{<k>} W_{ik} \tag{2.5}$$

Calling $\mathbf{P} \equiv (P_0, P_1, P_2, \ldots\ldots, P_N)$ (N is the total number of the particles in the system), the eq. (2.4) becomes

$$\frac{d\mathbf{P}(t)}{dt} = - \mathbf{H}\, \mathbf{P}(t) \tag{2.6}$$

and then formally

$$\mathbf{P}(t) = e^{-\mathbf{H}t}\, \mathbf{P}(0) \tag{2.7}$$

where $\mathbf{P}(0)$ represent the starting condition of the system. By using the Laplace transformation we obtain

$$\tilde{\mathbf{P}}(\varepsilon) = \int_0^{+\infty} dt\; e^{-\varepsilon t}\; \mathbf{P}(t) \;=\; \int_0^{+\infty} dt\; e^{-(\varepsilon + \mathbf{H})t}\, \mathbf{P}(0) \tag{2.8}$$

and with the initial conditions $P_i(0)=\delta_{i0}$ (at t=0 the diffusing particle is in the site 0)

$$\tilde{P}_0 (-\varepsilon + i\, 0^+) = \left[\frac{1}{\mathbf{H} - \varepsilon + i\, 0^+} \right]_{00} \tag{2.9}$$

and

$$-\frac{1}{\pi}\, \mathrm{Im}\, \tilde{P}_0 (-\varepsilon + i\, 0^+) = \left[\delta(\mathbf{H} - \varepsilon) \right]_{00} \tag{2.10}$$

Finally averaging over the N possible initial positions, we obtain the density

$$-\frac{1}{\pi}\, \mathrm{Im} <\tilde{P}_0(-\varepsilon + i\, 0^+)> = \frac{1}{N}\, \mathrm{Tr}\, \delta(\mathbf{H} - \varepsilon) \equiv \tilde{\rho}(\varepsilon) \tag{2.11}$$

It is clear that $\tilde{\rho}(\varepsilon)$ represents the density of the eigenvalues of $\mathbf{H}$ matrix. So that if we substitute the $\mathbf{H}$ matrix in eq. (2.11) with that of eq. (2.3) the immaginary part of the

Laplace transformation of $P_0(t)$ give us the density of the squared frequencies of the eigen modes of the structure. But, since we have that $\rho(\omega) = 2\,\omega\,\rho(\omega^2)$ then finally

$$\rho(\omega) = \frac{2\,\omega}{\pi}\ \mathrm{Im} <\tilde{P}_0(-\omega^2 + i\,0^+)> \qquad (2.12)$$

We have thus seen that the density of vibrational states can be obtained by solution of the coeeresponding diffusion problem on the structure.

2.3 Fractal structures and definition of spectral dimensionality

As stated in the previous chapter, random walk in a d-dimensional lattice has a fractal dimension d_W=2. This means that the average squared distance of a walker from the starting point scales with time as $<R^2> \sim t$. This equation, valid when t becomes large, can be taken as base of the definition of the diffusion coefficient $D = \frac{d<R^2>}{dt}$.

In general, when d_W assumes values different from 2 this coefficient has no significance, since it is no more a constant. In the case the fractal dimension of the random walk on a structure is different from 2 we will talk of "anomalous diffusion".

Let's thus think to a structure characterized by a fractal dimension $\bar{d}$ and a dimension d_W of the random walk on it. Concerning the probability $P_0(t)$ to find the walker on the origin of walk at time t, we can say that it will be proportional to the inverse of the number of distinct sites visited in the time t (i.e. S(t)), which is proportional to $R^{\bar{d}}$. Then

$$P_0(t) \sim S^{-1}(t) \sim R^{-\bar{d}} \sim t^{-\frac{\bar{d}}{d_w}} \qquad (t \to \infty) \tag{2.13}$$

where eq. (1.3) has been used (N has been substituted with t). The Laplace transformation of this equation gives

$$\tilde{P}_0(\varepsilon) \sim \varepsilon^{\frac{\bar{d}}{d_w}-1} \qquad (\varepsilon \to 0) \tag{2.14}$$

and finally from eq. (2.12)

$$\rho(\omega) \sim \omega \cdot \omega^{2\frac{\bar{d}}{d_w}-2} = \omega^{2\frac{\bar{d}}{d_w}-1} = \omega^{\tilde{d}-1} \tag{2.15}$$

We have thus obtained an expression for the density on vibrational states valid at low frequency for a fractal structure. The parameter $\tilde{d} = 2\bar{d}/d_w$ is the so called spectral dimensionality introduced originally by Alexander and Orbach[3] in 1982. This is an intrinsic parameter of the fractal structure because it depends only on the connectivity of the system.

2.4 Scaling arguments and decimation techniques

In this section we show how in some cases for non random self-similar structure by use of scaling arguments or RG, it is possible to calculate the dynamical exponents. As an example we will discuss the spectral dimension of the Sierpinski gasket.

We consider a fractal system characterized by the fractal dimensionality $\bar{d}$. Because of the self-similarity displayed by the system, under scale transformation by a factor *b*, the number of particles of the system related to the length L varies according to

$$N(b\,L) = b^{\bar{d}}\, N(L) \tag{2.16}$$

Correspondingly for the two structures (the original and that scaled by the factor b) the density of states for elementary unit, scales according to

$$\rho_L(\omega) = b^{\bar{d}}\, \rho_{L/b}(\omega) \tag{2.17}$$

If now we suppose that also the mode frequencies has a scaling behaviour such that

$$\omega(L/b) = b^{a}\, \omega(L) \tag{2.18}$$

the density of states must sutisfie the scaling relation

$$\rho_{L/b}(\omega) = b^{-a}\, \rho_L(\omega b^{-a}) \tag{2.19}$$

and by using eq. (2.17)

$$\rho_L(\omega) = b^{\bar{d}-a}\, \rho_L(\omega b^{\bar{d}-a}) \tag{2.20}$$

By setting $b = \omega^{1/a}$ finally we obtain

$$\rho(\omega) \sim \omega^{\frac{\bar{d}}{a}-1} \tag{2.21}$$

which the analogous of eq. (2.15). In this equation the parameter a has to be taken as equal to $d_W/2$.

As said above, in some case, the parameter a can be calculated by using renormalization techniques. These techniques are based on the fact that the scaling properties of the system give rise to scaling behaviour also for its dynamical quantities. In particular in the decimation procedures the dynamical quantities are calculated for scaled versions of the same systems and then they are compared to see if it is possible to extract the characteristic scaling low. To be clear, here we show an example of a decimation procedure to a Sierpinski gasket.[7]

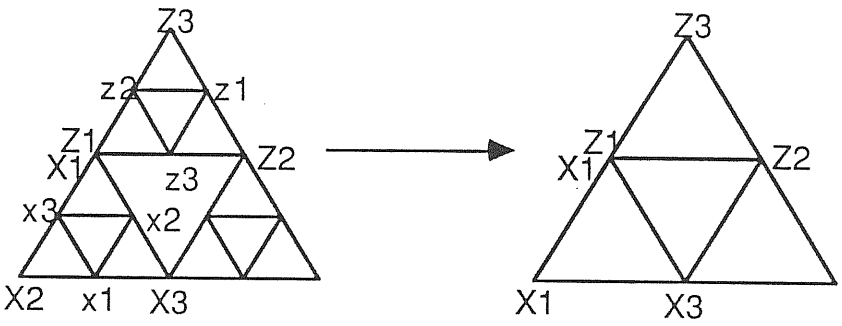

Fig. 2.1. Principle of the decimation procedure to derive the recursion relations for the elastic vibrations on a two-dimensional Sierpinski gasket.

Let's consider a Sierpinski gasket (see Fig. 1.3) in which identical masses m are located at the sites and joined by springs of strength K. Let us denote

$$\lambda = \frac{m\,\omega^2}{K} = \frac{\omega^2}{\omega_0^2} \tag{2.22}$$

the reduced squared frequency associated to the mode frequency ω.

The set of equations of motion for the mid-points of the lower left triangle (in Fig. 2.1) is:

$$\begin{aligned} \lambda x_1 &= \sum_{\delta} (x_1 - x_\delta) \\ \lambda x_2 &= \sum_{\delta} (x_2 - x_\delta) \\ \lambda x_3 &= \sum_{\delta} (x_3 - x_\delta) \end{aligned} \tag{2.23}$$

where δ denotes a neighbouring site of x_1 (resp. x_2, x_3).

The corresponding equation for X1 (or Z1) is:

$$\lambda X_1 = 4\,X_1 - (x_2 + x_3 + z_2 + z_3) \tag{2.24}$$

From eqs. (2.23) one can extract x1, x2 and x3 as function of $\{ X_i \}$ and the same for $\{ z_i \}$ as function of $\{ Z_i \}$. Inserting these values in eq. (2.24) one obtains a new equation where X_1 is a function of X_2, X_3 and Z_2, Z_3

$$\lambda(5-\lambda)\ X_1 = 4\ X_1 - (X_2 + X_3 + Z_2 + Z_3) \qquad (2.25)$$

This relation can be cast in the form of eqs. (2.23) with the renormalization[2]:

$$\lambda \rightarrow \lambda' = \lambda(5-\lambda) \qquad (2.26)$$

By this equation we can write the scaling relation for the vibrational frequencies of the two structures of Fig. 2.1, when $\omega/\omega_0 << 1$

$$\omega\left(\frac{L}{2}\right) = 5^{1/2}\ \omega(L) \qquad (2.27)$$

and finally, since the scaling factor b equals 2 the exponent a of eq. (2.18) is given by $a = \ln(5) / 2\ \ln(2)$. The spectral dimensionality of the Sierpinski gasket can now be evaluated by using eq. (2.21). Since $\bar{d} = \log3 / \log2 \approx 1.5849$ is the fractal dimension of the Sierpinski gasket, the spectral dimension results to be $\tilde{d} = 2\ \log3/\log5 \approx 1.3652$.

2.5 Long range forces and spectral dimensionality

Most of the existing exact and numerical results about diffusion and dynamical exponents of fractal systems were obtained by assuming first neighbor hopping bridges or interactions. On the other hand, one does not expect that further neighbor interaction can change the exponents, as long as the range of the forces remains finite.[8] In this respect, we sketch here briefly a simple model (see Ref.9) in which an exact renormalization method on a fractal allowing for long-range interactions was developed.

A triadic Koch curve (see Fig. 1.4), in which elastic forces, connecting the curve points at all length scales and following a self-similar scheme, were considered. The eigefrequencies of the resulting harmonic equations of motion were studied, in the limit of low frequency, with the use of a decimation procedure. This allowed the authors to obtain an explicit expression for the spectral dimensionality of the structure.

From the physical point of view, the model demonstrates that long-range forces radically change the spectral properties of the system and also lead to non universal dynamical critical behaviour. The results can be summarized in Fig. 2.2. Here the value of the spectral dimensionality has been plotted as a function of a parameter C which can be considered as determining the decay of elastic forces as function of distance R (i.e. $\alpha(R) \sim R^{\ln C/\ln 3}$, as $R \to \infty$).

We will mention again this model in chapter 4 in connection with the interpretation of some of our experimental results on low temperature relaxation of proteins.

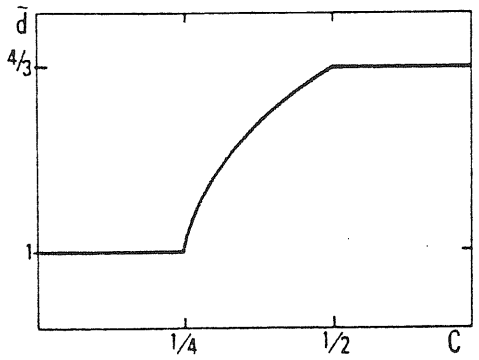

Fig. 2.2. Qualitative plot $\tilde{d}$ vs C.

References

1. P.G.de Gennes, *La Reserche*, 7, 919(1976)

2. H.J.Stapleton, J.P.Allen, C.P.Flynn, D.G.Stinson & S.R.Kurtz, *Phys.Rev.Lett.*, **45**,1456(1980)

3. S.Alexander & R.Orbach, *J. Phys.(Paris) Lett.*, **43**, L 625 (1982)

4. S.H.Liu, *Phys.Rev.*, **B 32**, 6094(1985)

5. C.Kittel, "Introduction to solid state physics", (Wiley & Sons, New York, 1966)

6. N.Go, T.Noguti & T.Nishikawa, *Proc.Natl.Acad.Sci.U.S.A.*, **80**,3696 (1983)

7. R.Rammal & G.Toulouse, *J. Phys. (Paris) Lett.*, **44**, L 13 (1983)

8. A.L.Stella, R.Dekeyser & A.Maritan, in *"Sixth Trieste International Symposium: Fractals in Physics"*, eds. L.Pietronero & E.Tosatti (North-Holland, Amsterdam, 1986)

9. A.Maritan & A.Stella, *Phys.Rev.*, **B 34**, 456(1986)

Chapter 3

Proteins: function, structure and dynamics

In this chapter we want to make a review of the main properties of proteins, both from the biological and the phisical point of view.

3.1 Protein function in the living systems

Proteins togheter with other molecules such as nucleic acids, are essential to the living systems. Their importance stems from the diversity of their functional roles. Such diversity can be easily illustrated by listing a few of the major groups within this molecular family.

Proteins are molecules that act to build the structural elements of organisms and to provide the energy necessary for life processes. Enzymes are proteins that catalyze biochemical reactions. Familiar examples include digestive enzimes that degrade foodstufs to simple, assimilable compounds, biosinthetic enzymes that build complex molecules from simpler compounds and muscle proteins that produce mechanical work from chemical reactions. Transport proteins such as hemoglobin facilitate the movement of molecular oxigen and other essential compounds to their sites of utilization.

Antibodies are proteins that bind to and neutralize foreign material that may be harmful for an organism. Other proteins are responsible for mantaining the structure of cells, organs and organisms, while still others play essential roles in genetic expression, nerve conduction and all other biological processes.

It is clear from the short panorama of the protein functions that this molecular family must be characterized by a large complexity. This obvious fact, is one of the peculiar features of protein molecules and it is also one of the aspects that limits a deep understanding of many of their properties. On the other hand, before analysing the dynamical aspects of protein motion in which we are particularly interested, it is important to have a correct idea of their structure.

3.2 Structure of proteins

Given the richness of proteins one would expect to observe a corresponding complexity in the detailed structure of these molecules. This expectation has been confirmed by X-ray diffraction studies, which have provided the crystal structure of more then 100 proteins during the past 25 years.[1,2]

Proteins are very large molecules; their molecular weights are often in the tens of thousands. The basic components of these molecules is the polypeptide chain, an unbranched polymer consisting of a sequence of amino acid residues. The structure of a short section of the polypeptide chain is illustrated in Fig. 3.1. The polypeptide chain is intrinsically flexible because many of the covalent bonds that occour in its backbone and sidechains are rotationally permissive. The primary limitation to the ranges of rotation for the backbone dihedral angles ϕ and ψ arise from nonbonded interactions.

That is, some values of ϕ and ψ are energetically unfavorable because lead to overlap of the repulsive cores of different atoms.

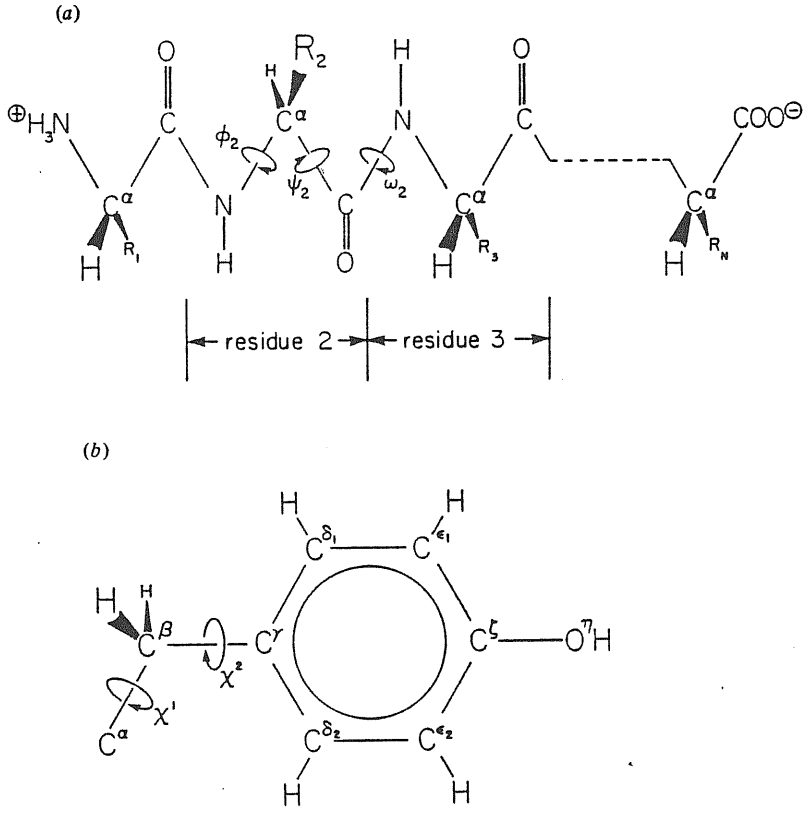

Fig. 3.1. Structure of the polypeptide chain. The backbone or main chain is shown in (*a*). The covalent bonds and bond angles and bond angles are rather rigid, but sizable rotations can occur *around* certain bonds. The dihedral angles ϕ_i and ψ_i measure the torsion about the rotationally permissive bonds in the backbone of residue *i*. The dihedral angles ω_i exhibit little variation because the C-N bond has partial double-bond character; each peptide group (CONH) and its adjoining C^{α} atoms therefore tend to remain in a common plane. The labels R_i represent the sidechains, one of which (a tyrosine sidechain) is shown in detail in (*b*). The tyrosine sidechain has two rotationally permissive bonds; the corresponding dihedral angles are χ^1 and χ^2. The ring remains relatively flat due to partial double bond character in its C-C bonds.

The residues of which the polypeptide is composed are chosen from the 20 commonly occurring amino acids. A given protein is characterized by a definite sequence of residues; this is usually termed the primary structure of the chain. The

amino acid residues are distinguished by the structures and chemical properties of their sidechains. The sidechains can be divided into two broad classes. Sidechains that are

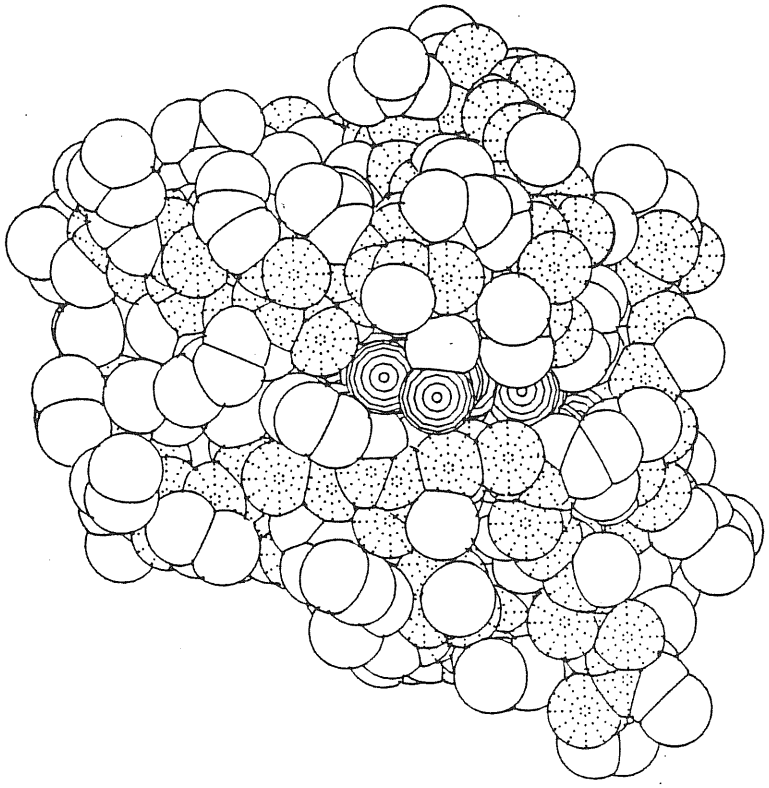

Fig. 3.2. Space filling representation of the native structure of a relatively small protein, cytochrome c. The sizes of the atomic spheres correspond to the distances of closest approach allowed by the core repulsion forces between nonbonded atoms.

relatively soluble in water are termed hydrophilic, while those that are less soluble in water are termed hydrophobic. The hydrophilic sidechains include electrically charged groups (acidic groups or basic groups, which typically bear a full negative or positive charge, respectively) and neutral groups with a substantial electrical dipol moment. The hydrophobic sidechains are neutral and relatively nonpolar.

The polypeptide chain of a given type of protein folds into a characteristic 'native' three dimensional structure in aqueous solution. For simple proteins, folding is a spontaneous process.[3,4] The atoms are packed quite densely in typical globular

proteins, so that the structures of these molecules can be described in terms similar to those used for dense liquids. Each group of covalently bonded atoms has a size and shape that can be described as a cluster of fused spherical cores (Fig. 3.2). The native structure then represents an efficient packing of these groups driven by their effective attractions for each other in the solvent surroundings.

The attractive interactions that determine protein structure include protein-solvent and solvent-solvent as well as protein-protein interactions (interactions between atoms or groups in the same protein molecule). Hydrophobic effects cause nonpolar sidechains to tend to cluster togheter in the protein interior. This effect is important because many of the residues in a typical protein are hydrophobic. On the other hand, charged groups in the protein will tend to occupy positions at the protein surface where they can enjoy maximal hydration.

The most prominent of the protein-protein acctractive interactions is hydrogen bonding.[5] Many groups in the polypeptide chain are potential donors or acceptors of hydrogen bonds. These include the peptide (CONH) groups in the backbone, and the sidechains of most of the hydrophilic residues. In the native structure, these groups must interact with one another in such a way that the loss of hydrogen bonds to the solvent water molecules is compensated by the formation of internal hydrogen bonds in the folding of the protein. For the protein backbone, such arrangements often result in the formation of what are termed elements of secondary structure. A familiar example is the alpha helix, in which the peptide oxigen of residue i forms a hydrogen bond with the peptide nitrogen of residue i+4 (Fig. 3.3(a)). Another example is the beta sheet structure, in which extended strands of the polypeptide chain lie next to one another and are cross-linked by hydrogen bonds between their peptide groups (Fig. 3.3(b)). Occasionally, one or a few water molecules occupy well-defined locations within proteins and serve as bridges between charged groups or hydrogen bond donors and

acceptors in the polypeptide. Groups that are not hydrogen bonded are attracted

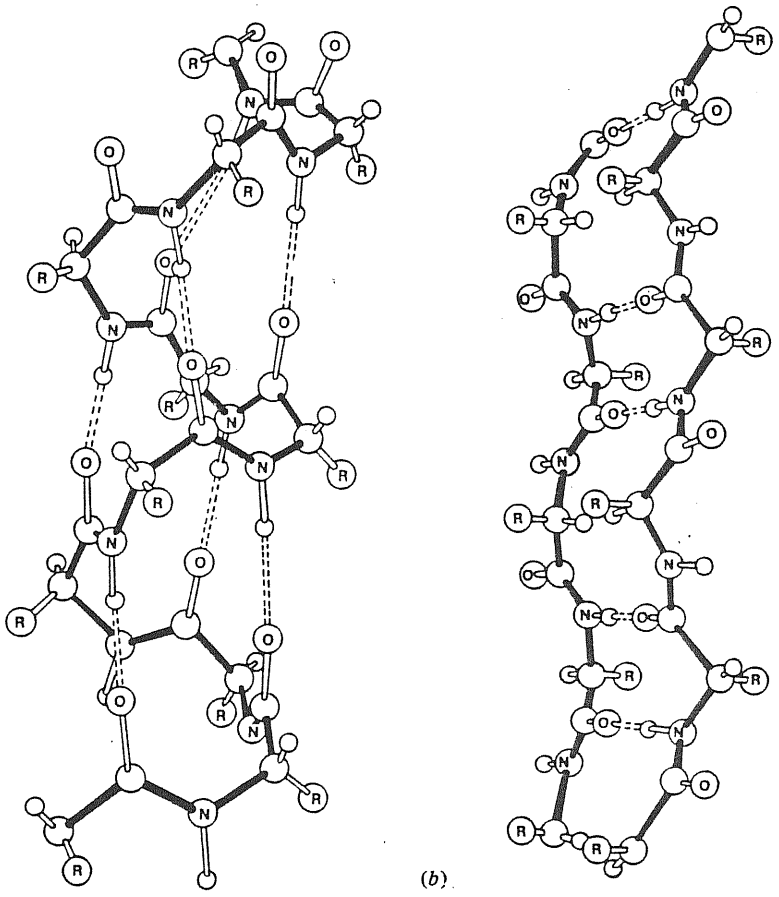

Fig. 3.3. Two types of secondary structures that are often observed in proteins. Both structures compensate for the loss of peptide-water hydrogen bonds upon folding by formation of peptide-peptide hydrogen bonds. (*a*) α helics. (*b*) Antiparallel β sheet.

togheter by weeker, less directional dispersion forces. These forces arises from the motion of the electrons about the atomic nuclei of each group. The istantaneous dipole moment of one such group of electrons and nuclei tends to polarize and thus attract the corresponding charges of nearby groups. For two methyl groups *in vacuo*, dispersion forces lead to a maximum stabilization on the order of 0.6 kJ/mol at a carbon-carbon distance of about 0.4 nm; reducing this distance by 0.1 nm results in a destabilization on the order of 10 kJ/mol due to core overlap. Although the maximum attractive dispersion interaction is one or two orders of magnitude weaker than that due to

hydrogen bonding, the former occurs among all the groups in a protein. Partly to compensate for the loss of dispersion interactions with solvent molecules in the folding process, the atoms in the protein interior tend to pack togheter quite closely.

The three dimensional arrengement of groups in the native protein is termed the tertiary structure of the molecule. This structure represents the optimum balance among the various interactions described above. Typical features include the clustering of hydrophobic sidechains in several regions of the protein interior. Charged sidechains tend to remain exposed to the solvent at the protein surface; the few charged groups observed in the protein interior are usually paired with oppositely charged groups. Sections of the polypeptide backbone that are buried in the protein interior typically form secondary structure to compensate for the loss of their hydrogen bonds with the solvent water molecules.

3.3 Protein dynamics

As illustrated in Fig. 3.1, a polypeptide chain consist of a large number of groups linked by covalent bonds that are intrinsically permissive of rotation. The groups linked by such bonds are themselves comparatively rigid and constitute the fundamental dynamical elements in a protein molecule. Examples of such groups are the CONH peptide groups that link successive residues, and the ring in the tyrosine sidechain. The typical thermal motions observed within a protein are dominated by the torsional oscillations of these groups about the single bond that link them togheter. Within such groups, only small atomic displacements occur due to the large energy cost of deforming bond lengths, bond angles and dihedral angles about multiple bonds. Superposition of rigid group displacements yields a remarkably rich dynamical

spectrum that ranges from the rapid local motions of the individual groups to slow collective distorsions of large regions within the molecule.

Because of the high packing density in the protein molecules, their atomic motion displays certain similarities to that seen in other dense materials. Over short periods of time (less then 0.5 ps), the small amplitude motions of the residues display similarity to the motions of molecules in a liquid. Each group is temporarily trapped, rattling in a cage that consists of other groups in the protein and (at the surface of the protein) molecules of the surrounding solvent. The cage atoms frequently collide with the encaged group, rapidly randomizing its motion. For many processes with longer characteristic times, types of motion that are typical of solid material appear. Such motions are expected, because the atoms of the protein have definite average positions corresponding to native molecular structure. Because of the interactions that mantein the structure, the protein matrix displays only limited compliance in the larger deformations that occur at long times. The solid-like aspects of protein behaviour appear on both local and global scales. Local group motions of large amplitude are typically opposed by substantial restoring forces associated with the distorsion of the cage surrounding the group. Consider, for example, the rotational isomerization of a tyrosine ring (Fig. 3.1) corresponding to 180^{o} change in χ^2. If the ring is located in the interior of a protein, a number of protein atoms are located in the volume that would be swept out by the ring during this rotation. The necessary displacement of these cage atoms associated with ring rotation produces substantial stress in the protein matrix; thus, there is a large energy barrier to the rotation of the ring. The underlying mechanism is similar to that which obtains for vacancy diffusion in crystals, i.e., hopping from one site to another with a strained intermediate state. In certain large scale motions, the distortion of the protein is distributed over many residues and the relative displacements of neighboring atoms are small. The protein can then be pictured as behaving somewhat

like a continous, elastic material. For a globular protein, one simple example would be a 'breathing' motion analogous to the fundamental mode of radial oscillation of a sphere.[6,7] Another example is the hinge bending motion that occurs in proteins having two globular regions that are linked by a region having a smaller cross section. In this type of motion, the protein may display a simple Hooke's-law character. Such motion typically display significant damping due to the solvent surrounding the protein. In addition to the local structural transitions and global elastic motions, proteins undergo more complicated global transitions on long time scales; these transitions have been compared to structural rearrangements that occur in glassy materials.[8-11] The native conformation of a protein comprises a large number of slightly different stable structures that correspond to different local minima in the potential energy surface of the system. Transitions among some of these substates are of direct biological importance. For example, the population of enzyme substates that have relatively high activity may be increased by the binding of e regulatory ligand. Many substates however, seem to exist as an accidental consequence of the composition of the protein; the extensive noncovalent interactions that stabilize the native canformation are tolerant of slight differences in how groups are packed togheter. The 'accidental' substates may be of indirect importance in biological function. For example, the redistribution of substates population upon binding of a regulatory ligand may be kinetically coupled to transitions among the accidental substates. Within a given protein, the energy barriers for such transitions appear to span a large range, from zero to tens of kJ/mol. The complicated, global character of many of these transitions is due to the dense packing of the residues in the protein. Rearrengement of packing in one region may depend on small rearrangements in neighboring regions, so that the transitions have a cooperative character. Good discussions of these issues have been provided recently by Ansari et al. and by Stein (see Refs 10 and 11).

As has been mentioned, both frictional forces and mechanical restoring forces play roles in the dynamic of proteins. The relative importance of these forces depence on the particular physical process considered. For local oscillations about a stable conformation, both underdumped and overdumped motions occur. Examples include underdumped of covalent bonds (a result of the large restoring forces togheter with the small size and correspondingly small frictional effects of the structural units involved), nearly damped oscillations of tyrosine rings relative to their cages,[12] and overdumped collective distorsion of hydrophobic cluster within a protein. Global distorsion of the hinge bending type are typically overdumped because of the large surface displacements and solvent dumping involved. A similar spectrum of behaviour obtains for structural transitions from one stable comformation to another. The rotation of tyrosine rings over the large barriers imposed by the protein matrix are of predominantly inertial character, although frictional effects reduce the rate of such transitions. Frictional effects are often dominant in transitions that involve large groups or smaller energy barriers. Simple examples include the rotation of sidechains at a protein surface (where the substantial restoring forces associated with a protein matrix are absent) and the unwinding of regions of the polypeptide chain from the protein surface (local denaturation).

3.4 New trends in structure and dynamics of proteins

The discussion we have done in 3.2 and 3.3 sections reflects the state of the studies on protein structure and dynamics conducted by experimental techniques and molecular dynamics calculations. The picture, emerging from the panorama of structural and dynamical characteristics of proteins above reported, is quite complicated and reflects the real complexity of these systems. Recently, as mentioned in the

introduction, also the ideas of fractals was used in the study of strcture and dynamics of proteins. We will analyse these concepts in the next chapter; in this chapter we will precise in more detail the connections between propei structure and dynamics presenting new experimental results on proteins and a new theoretical model for water nuclear relaxation as influenced by the protein fractal dynamics.

References

1. F.C.Bernstein, T.F.Koeltze, G.J.B.Williams, E.F.Meyer, M.D.Brice, J.R.Rodgers, O.Kennard, T.Shimanouchi & M.Tasumi, *J.Mol.Biol.*, **112**, 535 (1977)
2. J.S.Richardson, *Advances in Protein Chemistry*, **34**, 167 (1981)
3. C.Anfinsen, *Science*, **181**, 223 (1977)
4. T.E.Creighton, *J.Phys.Chem.*, **89**, 2452 (1985)
5. E.N.Baker & R.E.Hubbard, *Prog.Biophys.Mol.Biol.*, **44**, 97 (1984)
6. P.G.deGennes & M.Papoular, *"Polarization, Matiere et Rayonnement"*, Paris: Presses Universitaire de France (1969)
7. Y.Suezaki & N.Go, *International Journal of Peptide and Protein Research*, **7**, 333 (1975)
8. V.I.Goldanskii, Y.F.Krupyanskii & V.N.Flerov, *Doklady Biophysics*, **272**, 209 (1984)
9. J.A.McCammon, Rep. Prog. Phys., 47, 1 (1984)
10. A.Ansari, J.Berendsen, S.F.Browne, H.Fraunfelder, I.E.T.Iben, T.B.Sauke, E.Shyamsunder & R.D.Young, *Proc.Nat. Ac.Sci.USA*, **82**, 5000 (1985)
11. D.L.Stein, *Proc.Nat. Ac.Sci.USA*, **82**, 3670 (1985)

12. J.A.McCammon, P.G.Wolynes & M.Karplus, *Biochenistry*, **18**, 927 (1979)

Chapter 4

Fractal dynamics of proteins probed by electron and nuclear relaxation

Low frequency motion of biomolecules and more precisely proteins, is a relevant field of applicationof the concepts of fractal dynamics. In the next sections we will enter more deeply in these arguments by presenting some original experimental results on low temperature electronic relaxation of copper-containing protein Plastocyanin. Moreover a theoretical model for water nuclear relaxation in the presence of biomolecules based on their backbone fractal dynamics will be presented.

4.1 Low frequency protein vibrations and backbone fractal dynamics

Protein dynamics in nature can be considered as the most impressive expression of the close relationship between structure and function. In this respect, the role of collective, low frequency, motions appears of crucial importance in the catalytic activity of enzymes.[1] Over the last few years molecular dynamics simulations have provided a new insight into the characterization of the vibrational motion of small biological macromolecules.[2-4] On the other hand, the complexity of the algorithms and the

limitations imposed by computation time do not at present allow any complete and reliable analysis of the lowest vibrational modes occurring in large biomolecules.

4.1.1 Low temperature electronic relaxation time measurements and protein density of vibrational states

In the beginning of the eighties Stapleton and co-workers[5-8] proposed a new model for protein low temperature electronic relaxation in which an anomalous behaviour of the density of the vibrational states was used to explain the particular temperature dependence observed for the protein longitudinal electronic relaxataion time. In these works the proteins were thought as having a backbone structure typical of a self avoiding random walk but with the possibility of some extra connectivity probably due to hydrogen bonds or other kind of interactions present in proteins (see Chapt. 3).

Experimentally it was shown that many hemo-proteins, such as ferricytochrome c and cytochrome P-450, display an electronic relaxation time varying as a power of the temperature, when the latter is varied in the range 5÷15 K. In contrast with the expectations the exponents was found to have values close to 6.33. Since in the temperature range mentioned, Raman relaxation process is the most important in determining the relaxation time, connections with the density of the vibrational states were taken into account to explain that behaviour.

In the next sections a little summary on Raman relaxation process and a review of the Stapleton's results are presented. Moreover new experimental results on electronic relaxation of the copper-containing protein Plastocyanin will be presented as well.

a) The Raman relaxation process in proteins

Proteins, such as those mentioned above, contain a paramagnetic ion, Fe^{3+}, that can be directly detected by Electron Spin Resonance (ESR) giving a characteristic spectrum. In general, the paramagnetic ion is covalently bound to a certain number of ligands; the geometry of the resulting crystal field depends both on the ligands and on the electronic properties of the paramagnetic ion. Fe^{3+} ions in ferricytochrome c and cytochrome P-450 are bounded to four nitrogen atoms forming a planar structure. In these proteins the nitrogens togheter with Fe^{3+} are bound to the so called heme group.

Relaxation processes are due essentially to phonon-spin interactions mediated by the spin-orbit coupling. While in the direct process one have the absorption or the emission of a single phonon by the paramagnetic spin with energy matching the gap between the magnetic levels, in the Raman process the phonons are inelastically scattered. One can imagine in this case the process constituted by a two phonons process in which one is absorbed and the other emitted with the condition that the difference in energy between the phonons match the gap between the magnetic levels..

Physically, the relaxation process involves a modulation of the ligand electrostatic field by structural vibrations. This perturbs orbital electronic state that are coupled to the spin via the spin-orbit interaction. In general there are two contributions to a two-phonons relaxation rate. One comes from the use of first-order time-dependent perturbation theory and an orbi-lattice Hamiltonian, $\mathcal{H}_{OL}$, which is second order in strain (i.e. second order in phonon creation and destruction operator). The other arise from the use of second-order time-dependent perturbation theory with an orbit-lattice Hamiltonian, which is first order in strain. Only this second approach yields a non zero result for a Kramer's ion, because the $\mathcal{H}_{OL}$ operator is time even and therefore cannot connect the two states of a Kramer's doublet.

The features of the Raman relaxation rate can be reproduced by adopting the following simplified, phenomenological orbit-lattice Hamiltonian:

$$\mathcal{H}_{OL} = \sum_{l} \varepsilon \cdot V_l = \sum_{l\sigma} \left(\frac{\hbar \omega_\sigma}{2M\upsilon^2} \right)^{1/2} (b_\sigma - b_\sigma^\dagger) R_{l\sigma} V_l \qquad (4.1)$$

In this equation, ε is a strain operator and V_l is a time-even tensor operator that acts upon electronic wave functions and has, for simplicity, a single index l. $b_\sigma^\dagger$ and b_σ are the creation and destruction operators for phonons of index σ. $R_{l\sigma}$ is a dimensionless geometrical factor between a phonon of index σ and a tensor component V_l, but is independent of the phonon frequency ω_σ. M is the total mass and υ is the velocity at which vibrations propagate in the protein.

The relaxation rate is obtained as

$$1/T_1 = W(1 \rightarrow \bar{1}) + W(\bar{1} \rightarrow 1) \qquad (4.2)$$

where $W(n \rightarrow m)$ is the transition rate from $|n\rangle$ to $|m\rangle$ and $|1\rangle$ and $|\bar{1}\rangle$ are, in this case, the Kramer's conjugate states of the ground doublet. Since $W(1 \rightarrow \bar{1}) = W(\bar{1} \rightarrow 1)$ the relaxation rate becomes

$$\frac{1}{T_1} = \frac{4\pi}{\hbar} \sum_f \left| \sum_m \frac{\langle f|\mathcal{H}_{OL}|m\rangle\langle m|\mathcal{H}_{OL}|i\rangle}{E_i - E_m} \right|^2 \delta(E_i - E_f) \qquad (4.3)$$

where E_k is the energy of the state k.

The initial, intermediate and final states $|i\rangle$, $|m\rangle$ and $|f\rangle$ are each a product of electronic and phonon states. The intermediate phonon state can be created or destroyed in either order, then for a Kramer's ion there are four intermediate states to be included in the summation over m. So that the pertinent states are

$$
\begin{aligned}
|i> &= |1>|\ldots\ldots\ n_\mu,\ \ \ldots\ldots n_\lambda,\ \ldots\ldots\ > \\
|f> &= |\bar{1}>|\ldots\ldots\ n_\mu\text{-}1,\ \ldots\ldots n_\lambda\text{+}1,\ \ldots\ > \\
|m1> &= |j>|\ \ldots\ldots n_\mu\text{-}1,\ \ldots\ldots n_\lambda,\ \ldots\ldots\ > \\
|m2> &= |\bar{j}>|\ \ldots\ldots n_\mu\text{-}1,\ \ldots\ldots n_\lambda,\ \ldots\ldots\ > \\
|m3> &= |j>|\ \ldots\ldots n_\mu,\ \ldots\ldots\ldots n_\lambda\text{+}1,\ \ldots\ > \\
|m4> &= |\bar{j}>|\ \ldots\ldots n_\mu,\ \ldots\ldots\ldots n_\lambda\text{+}1,\ \ldots\ > \qquad (4.4)
\end{aligned}
$$

where n_μ is the thermal phonon occupation number $(e^{\hbar\omega/kT}-1)^{-1}$.

By considering the time reversal properties of the j's states we finally obtain

$$
\frac{1}{T_1} = \frac{\pi\hbar}{M^2\upsilon^4} \sum_{\mu\lambda} \omega_\lambda \omega_\mu n_\mu (n_\lambda+1) \Big| \sum_{j,l,l'} (R_{l\lambda}R_{l'\mu} - R_{l\mu}R_{l'\lambda}) \left(\frac{1}{\Delta_j - \hbar\omega_\mu} - \frac{1}{\Delta_j - \hbar\omega_\lambda} \right) <\bar{1}|V_l|j><j|V_{l'}|1> \Big|^2
$$

$$
\delta(\hbar\omega_\lambda - \hbar\omega_\mu - g\mu_B H) \qquad (4.5)
$$

where Δ_j is the energy of the jth excited Kramer's doublet.

In the limit of low frequencies the previous equation can be cast in the form

$$
\frac{1}{T_1} = \frac{4\pi\hbar^2}{M^2\upsilon^4} \sum_{l,l',j} \overline{\left(R^2_{l\lambda}R^2_{l'\mu} + R^2_{l\mu}R^2_{l'\mu}\right)}_{\lambda\mu} \left(|<\bar{1}|V_l|j><j|V_{l'}|1>|^2\right)/(\Delta_j^2)
$$

$$
\times \int_0^{\omega_{max}} \frac{\omega^4 \rho^2(\omega)\, e^{\hbar\omega/kT}}{(e^{\hbar\omega/kT} - 1)^2} d\omega \qquad (4.6)
$$

where the term $|R_{l\lambda}R_{l'\mu} - R_{l\mu}R_{l'\lambda}|^2$ has been now averaged incoherently over polarization and spatial index and removed from the summation over phonon modes appearing in eq. (4.5). Assuming for $\rho(\omega)$, the density of the vibrational states, the classical form

$$
\rho(\omega) \sim \omega^{d-1} \qquad (4.7)
$$

from eq. (4.6) the temperature dependence of the relaxation rate can be expressed in the form

$$\frac{1}{T_1} \sim T^{3+2d} J_{2+2d}(\Theta/T) \tag{4.8}$$

where $\Theta = \hbar\omega_{max}/k$ (the so called Debye temperature) and $J_n(x)$ is a transport integral defined as

$$J_n(x) = \int_0^x \frac{z^n e^z}{(e^z - 1)^2} dz \tag{4.9}$$

Eq. (4.8) well reproduce the dependence of Raman relaxation rates on temperature as observed in ordinary solids, i.e. d=3 (euclidean dimensionality), $T_1^{-1} \sim T^9$ at low temperature ($J_{2+2d}(\Theta/T)$ becomes a constant), $T_1^{-1} \sim T^2$ at high temperatures and $T_1^{-1} \sim T^9 J_8(\Theta/T)$ at intermediate temperatures. This behaviour generally valid for Kramer's ions, was also confirmed for covalently bound low-spin Fe3+ ion in the diamagnetic crystalline host $K_3Co(CN)_6$.[9,10]

It is clear, then, that under the conditions of validity of eq. (4.8) and generalizing the expression of the density of the vibrational states to that valid also for systems characterized by a fractal dynamics (see eq. (2.15)), the electronic Raman relaxation rate at low temperatures of a Kramer's ion, should behaves as the follows:

$$1/T_{1\ \text{electronic}} \sim T^{3+2\tilde{d}} \tag{4.10}$$

where $\tilde{d}$ is clearly the spectral dimensionality of the system.

b) Relaxation data on hemoproteins at low temperature

Stapleton and co-workers have collected a quantity of data on electronic relaxation at low temperature for several hemoproteins. They have shown that the relaxation of

these systems does not follow the temperature dependence expected for 3-dimensional

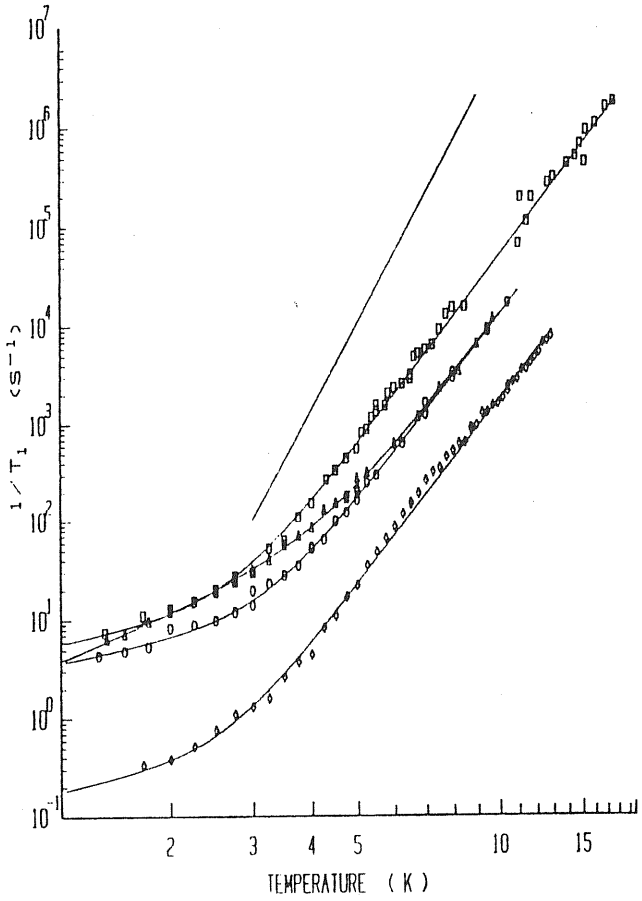

Fig. 4.1. Relaxation rate for low-spin hemoproteins. The data from cytochrome c (l, $1/T1 = 4.85T+0.0221T^{6.34}$), myoglobin (Δ, $1/T1 = 2.79T^2+0.007267T^{6.22}$), myoglobin azide (o, $1/T1 = 3.11T+0.0061T^{6.29}$), and P450 (◊,$1/T1 = 0.152T+0.000910T^{6.27}$) are separately fit to the sum of a direct process, varying with temperature as T or T^2, and a simple T^n power law. The best fitting values of n are indicated. Standard errors in n are tipically 1%. The straight line represents a T^9 power law.

objects and Kramer's ions (see previous section). Hemoproteins containing low-spin Fe^{3+} ion intrinsically display in fact an anomalous relaxation rate temperature dependence characterized by a slower Raman rate.

Fig. 4.1 shows some of the sets of data about some hemoproteins. From the figure one can see clearly the behaviour of the relaxation rate with temperature. The data fitted with a trial function of the form

$$f(T) = a\,T^{\alpha} + b\,T^{\beta} \qquad (4.11)$$

where the first term is needed to take into account the contribute to the relaxation of the direct process and the second for the Raman contribute, display Raman exponents β in the range 6.22-6.34. Data about other hemoproteins exhibited values of β also smaller then 6 but never higher than 7.[6] By using the consideration reported in the previous section, these values of β can be interpreted as evidence of a spectral dimensionality $\tilde{d}$ for the protein density of the vibrational states ranging between 1.4 and 2.

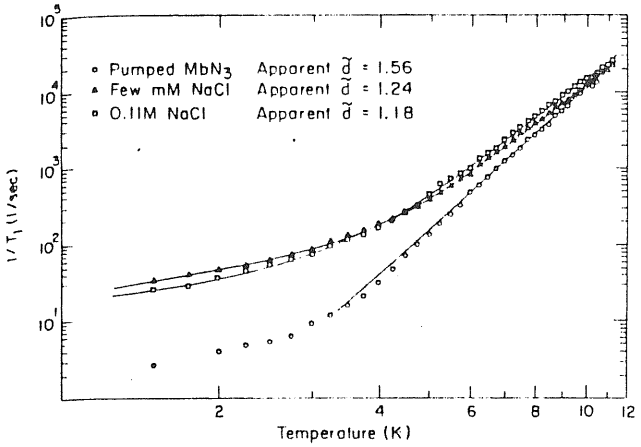

Fig. 4.2. Relaxation data from three samples of myoglobin azide under different solvent conditions.

The behaviour of the relaxation rate, in the Raman region, have also displayed a strong independence on sample hystory. It was also seen that the state of the sample does not influence the behaviour of the Raman relaxation rate; in this case only the direct process region is modified.[6]

However it is interesting to notice that appreciable influences on the Raman exponents were found when solvent conditions were changed (see Fig. 4.2).[7]

c) Relaxation data on copper-containing protein Plastocyanin

As reported in the previous section, hemoprotein relaxation data are generally characterized by the mentioned anomalous behaviour. It was, however, not completely clear if it had to be considered a general property of proteins or a peculiarity of the hemoproteins.

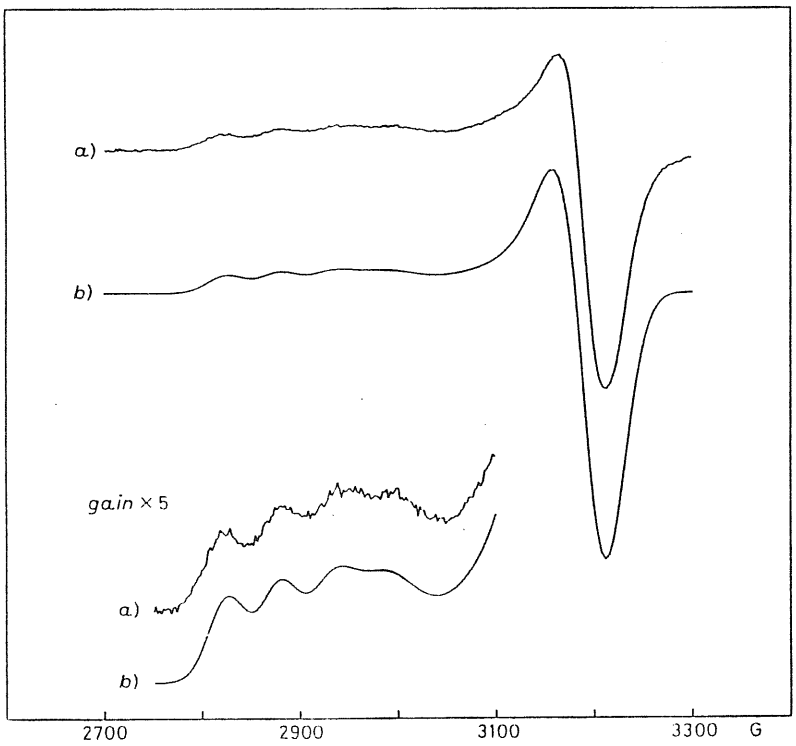

Fig. 4.3. Experimental (a) and computer-simulated (b) ESR spectrum of PC. The low-field part of the spectra is shown at fivefold higher gain. The experimantal spectrum was recorded at 77 K. The computed spectrum was generated by the theoretical model in refs. 11,12 and 13 with the following parameters: $g_{\parallel}$=2.251; $g_{\perp}$=2.047; $A_{\parallel}$=53.03 G; $A_{\perp}$=3.73 G; $LW_{\parallel}$=18.7 G; $LW_{\perp}$=21.11 G; $\sigma g_{\parallel}$=0.0074; $\sigma A_{\perp}$=8.85 G; ρ=1.

In this line, we report here the low relaxation data of the copper-containing protein Plastocyanin (PC) which can be used as evidence that the mentioned behaviour should be considered as a general characteristic of proteins. PC is a copper protein (molecular weigth about 10500) involved in the electron transport in photosyntesis. The intrinsic copper ion Cu^{2+} is bound to two nitrogen and two sulfur atoms supplyed by three different amino acid residues of the protein. The copper ion can be directly detected by Electron Spin Resonance (ESR) spectroscopy giving the characteristic spectrum shown in Fig. 4.3. In this figure is also reported the fitting of the experimental spectrum made by using the theoretical model reported in refs. 11,12 and 13. By this theoretical model

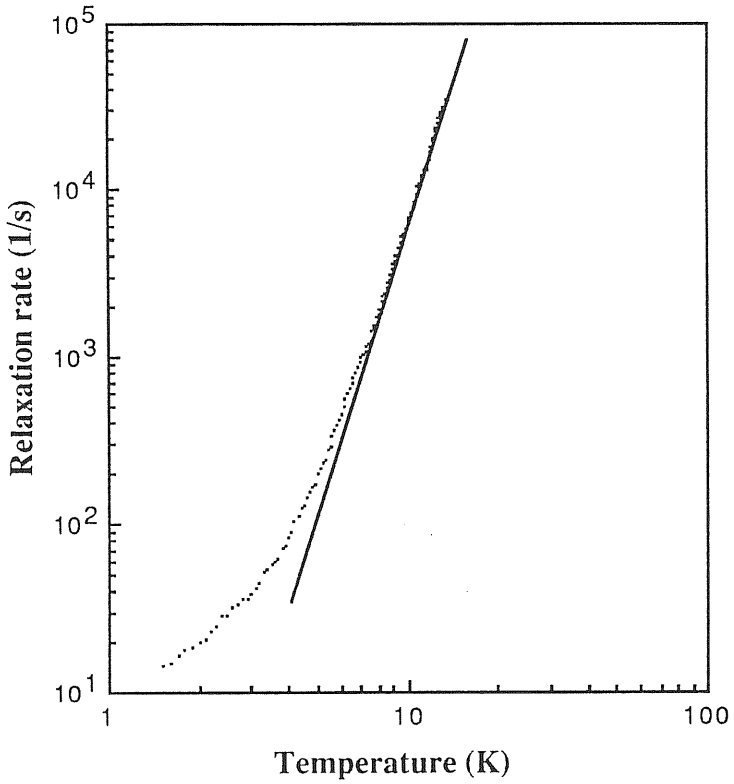

Fig. 4.4. Relaxation data of Plastocyanin. The streigth line in the figure represent a $T^{5.44}$ power law.

it was also suggested that the ESR spectrum shown in Fig. 4.3 is characterized by a statistical distribution of the spin hamiltonian parameters that should be due to small geometrical fluctuations in the crystal field.[12] Recently this fact was also interpreted as evidence of the presence of substates in the conformation of proteins.[14,15]

In Fig. 4.4 we report the relaxation data of low temperature aqueous solution of PC. As the figure shows the relaxation rate, in the Raman region, can be fitted with a power law $T^{5.44}$.The direct process region result in a linear temperature dependence. Following the method described above from the relaxation data is then extracted a value od 1.22 for the spectral dimensionality $\tilde{d}$.

d) Discussion

The experimental results on the relaxation of PC we presented here support the idea originally suggested by Stapleton that the anomalous behaviour of the low temperature relaxation of hemoproteins is not a particular property of this class of proteins but has to be considered as a typical property of all proteins. These results confirms also the fact that low frequency vibrational modes in proteins are characterized by fractal dynamical features. This idea was also supported by other authors[16] which suggested that in spite of the fact that the protein backbone constitutes a linear chain, extra connectivity due, e.g., to local bridges (e.g. hydrogen bonds) may confer to the structure a spectral dimensionality larger than 1. While there is general agreement on the importance of such bonds, there is considerable controversy about the specific mechanism by which they could affect the value of $\tilde{d}$.[17-19] In particular it has been shown by numerical simulation of diffusion on self-avoiding chains, that $\tilde{d}$ stays equal 1 if the crosslinks are assumed to be short-range.[20] Moreover it was suggested that the values of $\tilde{d}$ found

for proteins may be due to the presence of long-range forces which should be definitely considered as responsible for values of the spectral dimensionality grater than 1 (see section 2.5 and ref. 21). In proteins long or infinite range forces can be provided by salt bridges (i.e., weakly screened Coulomb forces) or by effects of elastic distorsion of the surrounding frozen solvent. This point is also in agreement with the experimental findings (already mentioned in sec. 4.1.1 b)) about the influence of solvent conditions on the Raman relaxation behaviour of proteins.

In connection with this issue, we should extend our discussion. It is our convinction that the role of the embedding solvent has not been sufficiently considered up to now and could be a clue to a better understanding of the experiments. We think that considering the proteins as a fractal structure completely decoupled from the solvent is a too drastic schematization. The biomolecule should be rather viewed as a kind od "defect" embedded in the bulk of the frozen solvent. We are presently engaged in a very extensive investigation of how this situation affects the fractal dynamics of the protein in very simplified models.

In practice we consider a fractal backbone (i.e. a square Koch curve) inserted in square lattice. Elastic forces along the backbone and connecting the fractal to the lattice are considered. The frequencies and the ampitude of the vibrational modes are then calculated by using numerical methods as those reported in secs. 2.1 and 2.2. With these calculations the main purpose is that to obtain the shape of the density of vibrational states for the fractal togheter with the amplitude of the modes.

The preliminary results we obtained seem to support the idea that the presence of the solvent-fractal interactions can introduce into the fractal, vibrations that can radically change its original spectral properties. In particular we have seen that, for the calculations we have done by considering fractals of different sizes, the density of vibrational states seems to be characterized by a cross-over between a region displaying

bulk-density features and another at higher frequency, which is fractal in character. These results have to be considered as preliminar, but further progress is expected in the near future along these line.

4.1.2 A theoretical model for nuclear relaxation of water in the presence of protein molecule based on a fractal dynamics protein backbone

Since the presence of biomolecules considerably enhances the solvent water proton relaxation rate, NMR relaxometry has been considered appropriate for gaining direct experimental access to their elementary backbone dynamics.[22,23] Knowledge of this type moreover, deserves great interest from the application standpoint, because most of the contrast observed in NMR imaging is determined by the water proton relaxation times. Certain models that attribute water relaxation times to either the rotational or the translational correlation times of the biomolecules have been also proposed.[24,25] Nevertheless, a suitable relaxation theory that connects the NMR relaxation behaviour with biopolymer dynamics and that is consistent with the experimental results has yet to be formulated.

We here report a theoretical model in which the NMR relaxation profiles of biopolymer water solutions are interpreted in terms of the magnetic field fluctuations arising from the backbone motion involving the biopolymer paramagnetic nuclei. In this model we have taken into account the experimental evidence in the literature[5-8,26] for a "fractal-like" behaviour for the backbone dynamics of proteins. The model has allowed us to obtained very good fits of several experimental NMR relaxation dispersion profiles from aqueous solutions of biomolecules.

a) The theoretical model

The conventional theory of NMR relaxation,[27] in which the magnetic field fluctuations are characterized by the time correlation function $<H_i(0)H_i(t)>=<H_i^2>e^{-t/\tau}$ with a single correlation time τ, provides the following dipolar relaxation rate for water protons (we will consider, for simplicity, the longitudinal rate $1/T_1$, but similar results could be obtained for $1/T_2$ and $1/T_{1r}$):

$$\frac{1}{T_1} = \frac{2}{3}\gamma^2 <H_i^2> \frac{\tau}{1+\omega^2\tau^2} \qquad (4.12)$$

γ is the proton gyromagnetic ratio, ω is the angular frequency corresponding to the NMR resonant frequency of water protons and $<H_i^2>$ is the mean square value of the fluctuating magnetic field $H_i(t)$ experienced by the water protons. The usually low NMR relaxation rate exhibited by bulk water protons is attributable to motional narrowing effects due to the fast rotational diffusion ($\tau = 10^{-12}$ s) of water molecules.[27] This situation, which can be expressed in eq.(4.12) by putting $\omega\tau << 1$, leads to T_1^{-1} being independent of the frequency. In aqueous solutions, water molecules hydrated to biomolecules are in rapid exchange with water molecules in the bulk. The relaxation rate is, then, a weighted average of the two fractions of water:

$$\frac{1}{T_1} = \frac{x}{T_{1b}} + \frac{1-x}{T_{1f}} \qquad (4.13)$$

where x is the mole fraction of bound (b) water and 1-x is the fraction of free (f) water. Since x is very small, T_{1b} must be brought down by several orders of magnitude from T_{1f} for the overall change in the observed T_1 to be significant. In this respect, one can imagine that the overall vibrational motion of a biomolecule, resulting from thermal activation of its characteristic vibrational modes, allows each paramagnetic nucleus of its backbone and side chains to become a source of fluctuating magnetic field.[22,23] The

water protons around the protein molecules (bound water) will then explore a distribution of fluctuating magnetic fields which is determined by the intrinsic characteristics of the protein dynamics. The bulk water is then coupled to the relaxation mechanisms by rapid diffusion and exchange or cross-relaxation.[22-25]

As concerning the dynamic features of these systems in the line of the ideas reported in the previous section we assume the density of states for the backbone vibration to have the form

$$\rho(\nu) \sim \nu^{\tilde{d} - 1} \tag{4.14}$$

where now $\tilde{d}$ is the well known spectral dimensionality that for proteins was found in the range 1.2÷1.7. Under this hypotesis the density of staes deviate considerably from the classic form $\rho(\nu) \sim \nu^2$. These experiments have provided strong support for the hypothesis that proteins could be modelled by self avoiding random walks (see section 4.1.1) with some connectivity[19] and behaving as a fractal network whose dynamics has been characterized by a spectral dimensionality.[29] In this connection, we assume a "fractal-like" dynamics for the biomolecules.

We should then expect each vibrational mode to be characterized by a correlation time τ which can be related to the frequency of the mode by the relationship provided by Orbach and co-workers: [30]

$$1/\tau \sim \nu^{6 - 4\tilde{d}}\, \rho(\nu) \tag{4.15}$$

The assumptions made so far lead to the presence, in our systems, of a distribution of fluctuating fields characterized by a distribution of correlation times $g(\tau)=\rho(\nu)|\, d\nu/d\tau|$, which can be worked out from eqs. (4.14) and (4.15) The total water proton relaxation rate due to all the protein vibrations will then be expressed by the following integral:

$$R_{1p} = \frac{2}{3}\,\gamma^2 \int_{\tau_{min}}^{\tau_{max}} H_M^2(\tau)\, g(\tau)\, \frac{\tau}{1+\omega^2\tau^2}\, d\tau \qquad (4.16)$$

where τ_{min} and τ_{max} are the lower and upper limits of the correlation time distribution, respectively. $H_M{}^2(\tau)$ is now the mean square value of the fluctuating magnetic fields associated with the vibrational modes of correlation time τ, averaged over all the paramagnetic nuclei of the protein molecule (due to its rapid drop with r its value could be significant only for the first hydration layer). With considerations similar to those reported in ref. 22 we found that $H_M{}^2$ shows a slight dependence on τ. If, finally, we take into account the small relaxation rate of the free water protons R_{1w}, as already mentioned, the overall water proton relaxation rate of biomolecule water solutions turns out from eqs. (4.14), (4.15) and (4.16), to be:

$$\frac{1}{T_1} = R_1 = R_{1w} + R_{1p} = R_{1w} + C \int_{\tau_{min}}^{\tau_{max}} \frac{\tau^{-\tilde{d}/(5-3\tilde{d})}}{1+\omega^2\tau^2}\, d\tau \qquad (4.17)$$

where C is a constant proportional to $H_M{}^2$ which has to be evaluated, for each set of experimental data, by a fitting procedure.[31]

b) Results and discussion

Eq.(4.17) has been used to fit several NMR relaxation dispersion profiles of biomolecule water solutions reported in the literature. As examples, in Figs.4.5 and 4.6 we show the best fits of the longitudinal relaxation rate as a function of the NMR frequency obtained for hemocyanin (experimental data are from ref.24) and mouse

muscle (data from ref.25) water solutions, respectively. In these figures we have also

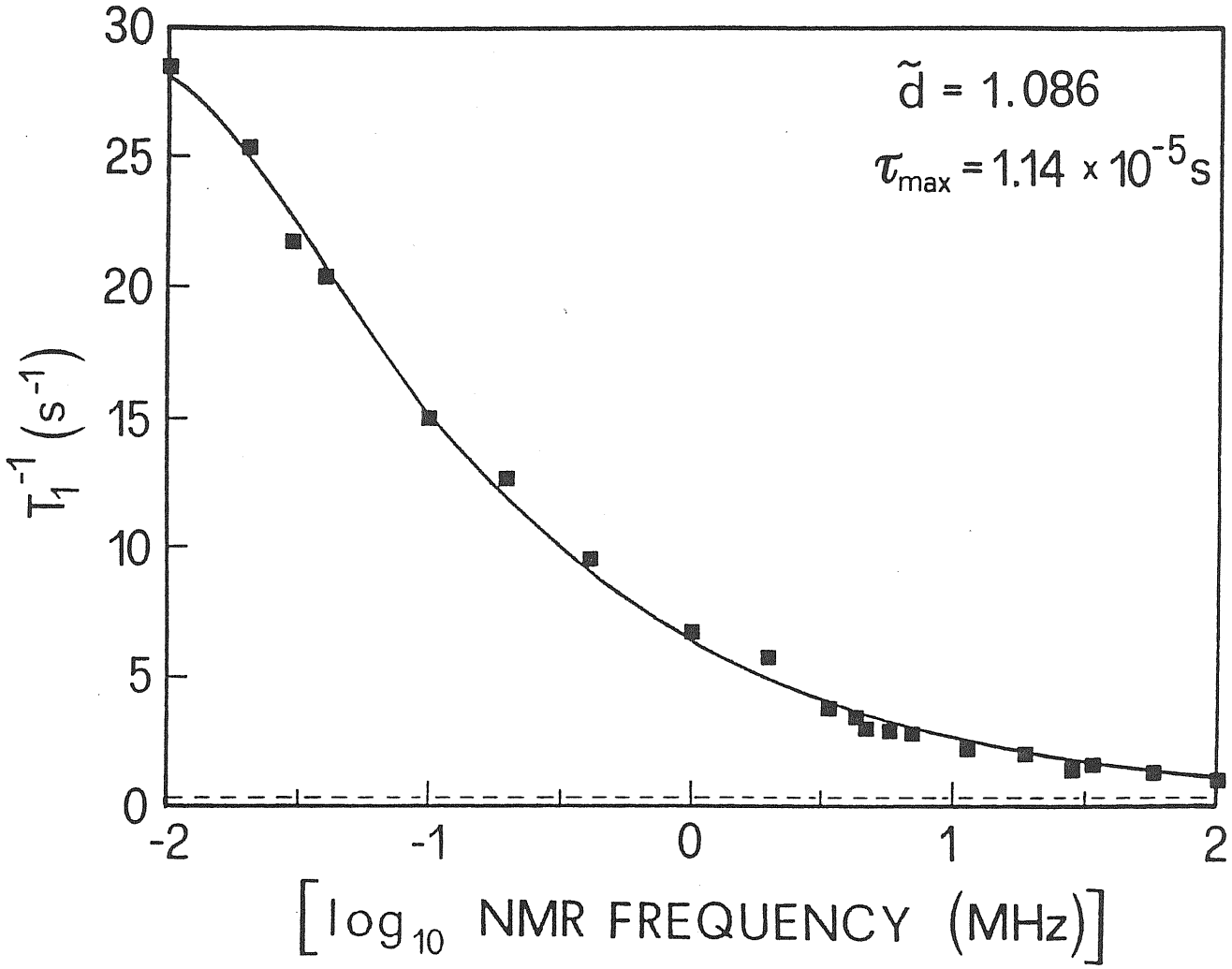

Fig. 4.5. Relaxation rate as a function of NMR frequency for water solution of hemocyanin. The experimental points are from ref.24. The full line is from our dynamical model. The relaxation rate of the free water protons (R_{1w}) is indicated by the dashed line.

The values of $\tilde{d}$ and τ_{max} heve been determined to a precision of 0.5 and 1.0 % respectively.

reported the related values of $\tilde{d}$ and τ_{max} which resulted from the best fitting procedure. τ_{min} was fixed in all the fits to a value of 10^{-13} s according to the correlation time values obtained by molecular dynamic calculations[4] for the highest

frequency modes; on the other hand, the evaluation of the integral appearing in eq.

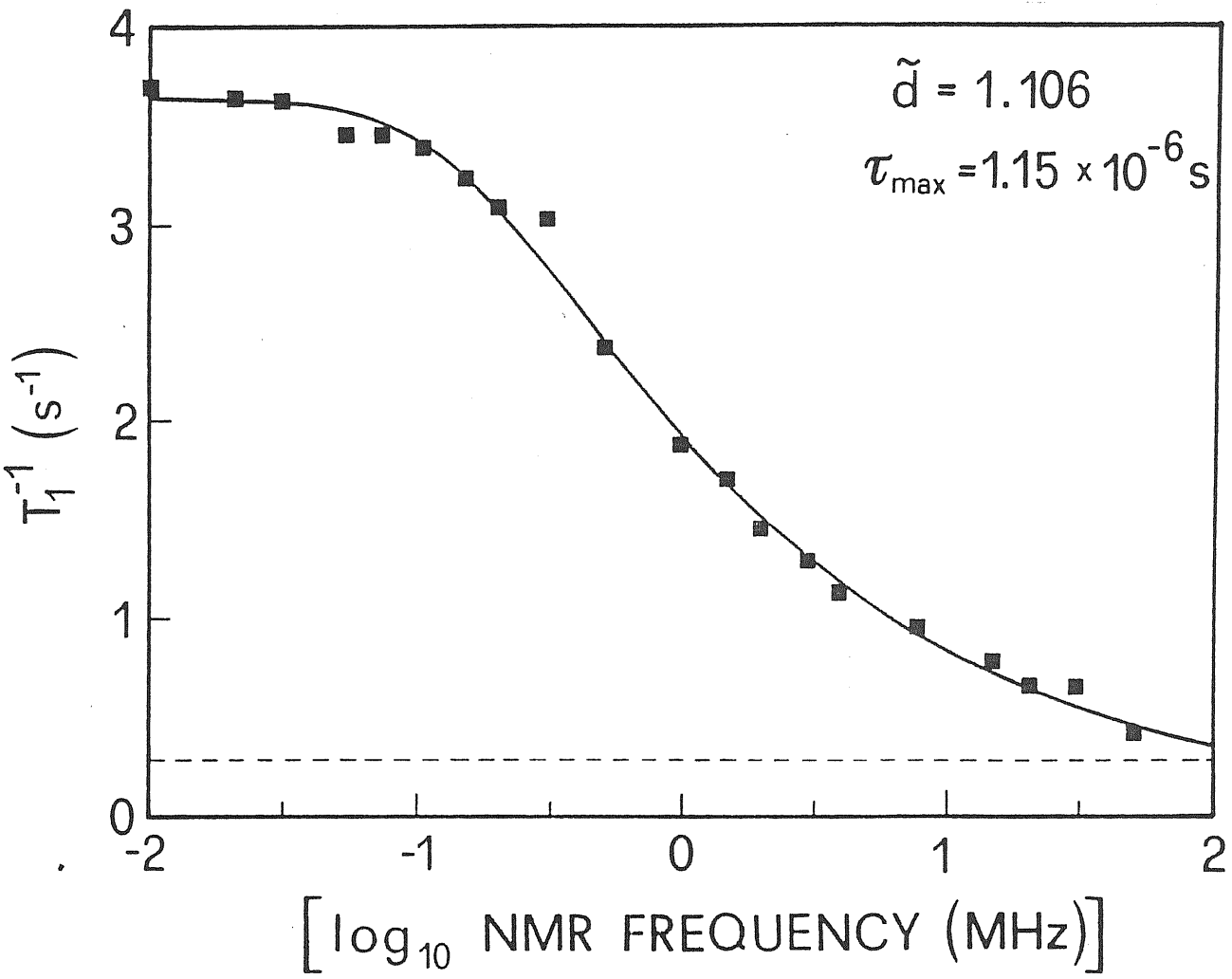

Fig. 4.4 Relaxation rate as a function of NMR frequency for mouse muscle. The experimental points are from ref. 25. The full line is from our dynamical model. See also the legend of Fig. 4.4.

(4.17) is practically independent of τ_{min} when its value is lower than 10^{-10} s. From the goodness of the fits obtained, it can be inferred that the theoretical model proposed is able to reproduce quite well the experimental behaviour of the longitudinal relaxation rate as a function of the NMR frequency of aqueous solutions of biomolecules. The values obtained for the spectral dimensionality $\tilde{d}$, which ranged from 1.0 to 1.2, for

the different biomolecules, indicate that the biomolecule backbone is undergoing a fractal dynamics which differs slightly from that of linear polymers (some connectivity between chain sites may be provided by hydrogen bonds[16]). Go and co-workers[3] have calculated the vibrational modes of a small protein, the bovine pancreas trypsin inhibitor, in vacuo. They found a range of 150 - 3600 GHz for the frequencies associated with the collective vibrational modes of the protein backbone. On the other hand, these modes have been shown[8] to provide a density of states of the form hypothesized for fractal networks. Now, if we assume that the maximum value of the frequency (3600 GHz) is associated to the lowest correlation time ($\tau_{min}=10^{-13}$ s),[2,4] eq. (4.14) can be turned into a quantitative relation and a correspondent frequency can then be associated to each value of τ_{max} obtained by the fits, provided that the related value of $\tilde{d}$ is used. For the two cases shown in Figs. 4.4 and 4.5, frequency values of 0.228 and 0.085 GHz are obtained. Even if the protein systems compared are different, this estimation of ν_{min} seems, to within the framework of the model, to indicate that collective modes at lower frequencies than those calculated in vacuo are contributing to the NMR relaxation in water solutions. These results are in agreement with other authors[32,33] who have argued for the existence of vibrational motion at frequencies much lower than those obtained by molecular dynamics calculations and other theoretical methods.[3,4]

If the biopolymer dynamics mechanism is a correct description of the relaxation of water in biopolymer solutions, NMR relaxometry can provide much useful information on the dynamical aspects of these systems. For instance, the lowest frequency modes of their backbone are accessible and can be characterized under NMR experimental conditions that are very close to the biological ones. The most noteworthy result is however that the spectral dimensionality, indicating a "fractal-like" vibrational density of states for these systems, can be estimated.

References

1. J.A.McCammon, B.R.Gelin & M.Karplus, *Nature(Lond.),* **262**,325(1976)
2. S.Swaminathan, T.Ichiye, W.van Gunsteren & M.Karplus, *Biochemistry,* **21**, 5230(1976)
3. N.Go, T.Noguti & T.Nishikawa, *Proc.Natl.Acad.Sci.U.S.A.,* **80**,3696(1983)
4. J.A.McCammon, *Rep.Prog.Phys.,* **47**,1(1984)
5. H.J.Stapleton, J.P.Allen, C.P.Flynn, D.G.Stinson & S.R.Kurtz, *Phys.Rev.Lett.,* **45**,1456(1980)
6. J.P.Allen, J.T.Colvin, D.G.Stinson, C.P.Flynn & H.J.Stapleton, *Biophys.J.,* **38**,299(1982)
7. J.T.Colvin & H.J.Stapleton, *J.Chem.Phys.,* **82**, 4699(1985)
8. G.C.Wagner, J.T.Colvin, J.P.Allen & H.J.Stapleton, *J.Am.Chem.Soc.,* **107**, 5589(1985)
9. T.Bray, G.C.Brown & A.Kiel, *Phys.Rev.*, **127**,730(1962)
10. A.Rannestad & P.E.Wagner, *Phys.Rev.*,**131**,1953(1963)
11. G.Giugliarelli & S.Cannistraro, *Chem.Phys.*, **98**, 115(1985)
12. S.Cannistraro & G.Giugliarelli, *Mol.Phys.*, **58**, 173(1986)
13. C.X.Wang, G.Giugliarelli & S.Cannistraro, *Nuovo Cimento D*, **8**, 76(1986)
14. H.Fraunfelder, in "Amorphous and liquid materials", E.Luscher, G.Fritsch & G.Jacucci eds. (Martinus Nijhoff Publ., Dordrecht, 1987)
15. G.Giugliarelli & S.Cannistraro, IX Congresso Gruppo Nazionale di Cibernetica e Biofisica, Trento 23-25 September 1988, Abstract Book p.227

16. J.S.Helman, A.Coniglio & C.Tsallis, *Phys.Rev.Lett.*, **53**,1195(1984)

17. M.E.Cates, *Phys.Rev.Lett.*, **54**, 1733(1985)

18. H.J.Stapleton, *Phys.Rev.Lett.*, **54**, 1734 (1985)

19. J.S.Helman, A.Coniglio & C.Tsallis, *Phys.Rev.Lett.*, **54**, 1735 (1985)

20. A.L.Stella, R.Dekeyser & A.Maritan, in *"Sixth Trieste International Symposium: Fractals in Physics"*, eds. L.Pietronero & E.Tosatti (North-Holland, Amsterdam, 1986)

21. A.Maritan & A.Stella, *Phys.Rev.* **B 34**, 456(1986)

22. H.E.Rorschach & C.F.Hazlewood, *J.Magn.Reson.***70**,79(1986)

23. R.Kimmich, F.Winter, W.Nusser & K.H.Sphon, *J.Magn.Reson.***68**,263(1986)

24. K.Hallenga & S.H.Koenig, *Biochemistry* **15**,4255(1978)

25. B.M.Fung, *Biophys.J.***18**,235(1977)

26. M.Bacci & S.Cannistraro, *J.Chem.Faraday Trans.***83**,(1987)

27. C.P.Slichter,*"Principles of magnetic resonance"*, Berlin, Springer Verlag,(1978)

28. B.B.Mandelbrot,*"The fractal geometry of nature"*, San Francisco,W.H.Freeman, (1982)

29. S.Alexander & R.Orbach, *J.Phys.Lett.***43**,L625(1982)

30. A.Aharony, S.Alexander, O.Entin-Wohlman & R.Orbach, *Phys.Rev.Lett.***58**, 132(1987)

31. An explicit expression for C can be worked out by taking into account its dependence on H_M^2, the total number of water molecules, N_{bw}, in the biopolymers hydration shell, the degrees of fredom, N_g, (to include in the normalization of $\rho(\nu)$), the frequency nmin and the correlation time tmax (see section 4.1.2.b) of the biopolymer. The obtained formula

$C = 2\,\gamma^2\, N_g\, H_M^2\, N_{bw}\, \tilde{d}\, \nu_{max}^{5-2\tilde{d}} \,/\, 3\,|5-3\tilde{d}|\, \tau_{min}$ can be used to estimate H_M once C

has been obtained from the fit. In the case reported in Fig. 4.3, a value of about 0.02 Gauss resulted for H_M. Such a value appears quite realistic and is of the same order of that obtained by using for H_M the expression reported in ref. 9.

32. B.N.J.Persson, *Chem.Phys.Lett.***127**,428(1986)

33. M.J.Bogusky, R.A.Schiksnis, G.C.Leo & S.J.Opella, *J.Magn.Reson.* **72**,186(1987)

Chapter 5

Fractal surfaces: numerical evaluation of random walk exponents

The discussion of solvent effects in the last chapter (see sec, 4.1.1. d)) is an example of the possible usefulness of a modellistic, computational approach to spectral properties as far as the qualitative understanding of protein experiments is concerned. Another example of this usefulness is the discussion of the effect of long-range forces reviewed in sec. 2.5.

We are convinced that further progress in the study of protein dynamics will require, among many other things, a more extensive use of, at least qualitative models and simulations. In particular we are at present developing an extensive program of simulation in order to better understand the effects of the embedding solvent on the dynamics of fractal structures.

To be involved in such theoretical programs opens an easy way to attach with similar methods also other issues, not directly connected with electronic or nuclear relaxation in proteins, but more generally belonging to the broad field of fractal dynamics and to areas related to it, e.g. polymer or menbrane statistics.

A part of the work reported in this thesis is indeed concerned with a problem (the spectral properties of a fractal surface) which is also connected with the statistics of menbrane models. (Another application of the results of this chapter could be the

description of, e.g., biocatalytic processes occurring at the boundary of large enzymes[1]). In the next sections we will discuss the calculation of the spectral and diffusive exponents of a specific fractal surface.

5.1 Fractal surfaces

Random and fractal surfaces are interesting in condensed matter physics, where, e.g., one may wish to describe the behaviour of rough interfaces[2] or polymeric membranes. They are also important in particle physics, because of the close relations between theories of self-interacting surfaces and string theories or lattice gauge theories.[3-5]

From a statistical point of view random surfaces (RS) in d-dimensional spaces display properties that are not yet understood completely. In the limit $d \rightarrow \infty$ it has been shown[6] that the radius of gyration R varies as a power of N (number of plaquettes of the surface, when the surface is defined on a lattice) with an exponent $\nu = 1/4$. For finite d, the ν exponent of self-avoiding-surfaces (SAS) is expected to vary as $\nu = 3/(4+d)$ when $d \leq 8$ and $\nu = 1/4$ for d larger than 8. This result was obtained by using a Flory approach[7] with the assumption that SAS do not display tubular, tree-like configurations as the dominant ones. For this latter case a more appropriate value of ν should be the one pertaining to branched polymers, $\nu = 5/2(d+2)$.

In view of the complexity of the problem, up to now, few numerical calculations have been performed. Moreover, contradictory results exist in the literature. While Glaus and Einstein[8] seem to favour definitely a branched polymer-like value for d=3 ($\bar{d} = \nu^{-1} \approx 2$), Karowsky[9] gave recently support for a value $\bar{d} = 2.30 \pm 0.05$ which would be compatible with the formula reported above ($\bar{d} \approx 2.33$).

A more definitive understanding of the properties of SAS on a lattice remains for the moment a big analytical and numerical challenge. SAS's on a lattice have the possibility of branching, because the connectivity of each site is not fixed. These models are thus not very suitable for representing physical situations where, the connectivity at each site is fixed, like in a preassigned network. This is a realistic feature in problems like membranes, sheet polymers, etc.....

The study of surfaces with fixed connectivity may also have a more direct application to the study of the conformations of real molecular surfaces.[1,2] It is recent, in fact, the evidence that also protein surfaces at the molecular level display self-similar properties in a length range wide enough to be characterized by a fractal dimension $\bar{d} = 2.17 \pm 0.02$.[1] Therefore, in spite of the fact that the study of random and fractal surfaces deserves its own importance in several other fields, it may be also relevant in the understanding of properties and functions of such biomolecules.

5.1.1 Fractal surfaces and random walks

a) <u>The hydrant fractal surface</u>

We have considered the fractal surface called "hydrant" shown in Fig. 5.1. As it can be easily verified, this surface have a fractal dimensionality $\bar{d} = \log 13/\log 3 \approx 2.3347$.

As concerning the random walk on the surface, let us imagine a walker placed in one of the plaquettes of the surface. Looking at the Fig. 5.1, t can jump in the plaquettes will have a side in common with that where it is currently placed. However, it cannot jump in such kind of plaquettes, if these are in buildings of the surfaces different from that to which its current plaquette belongs. The coordinates of the current

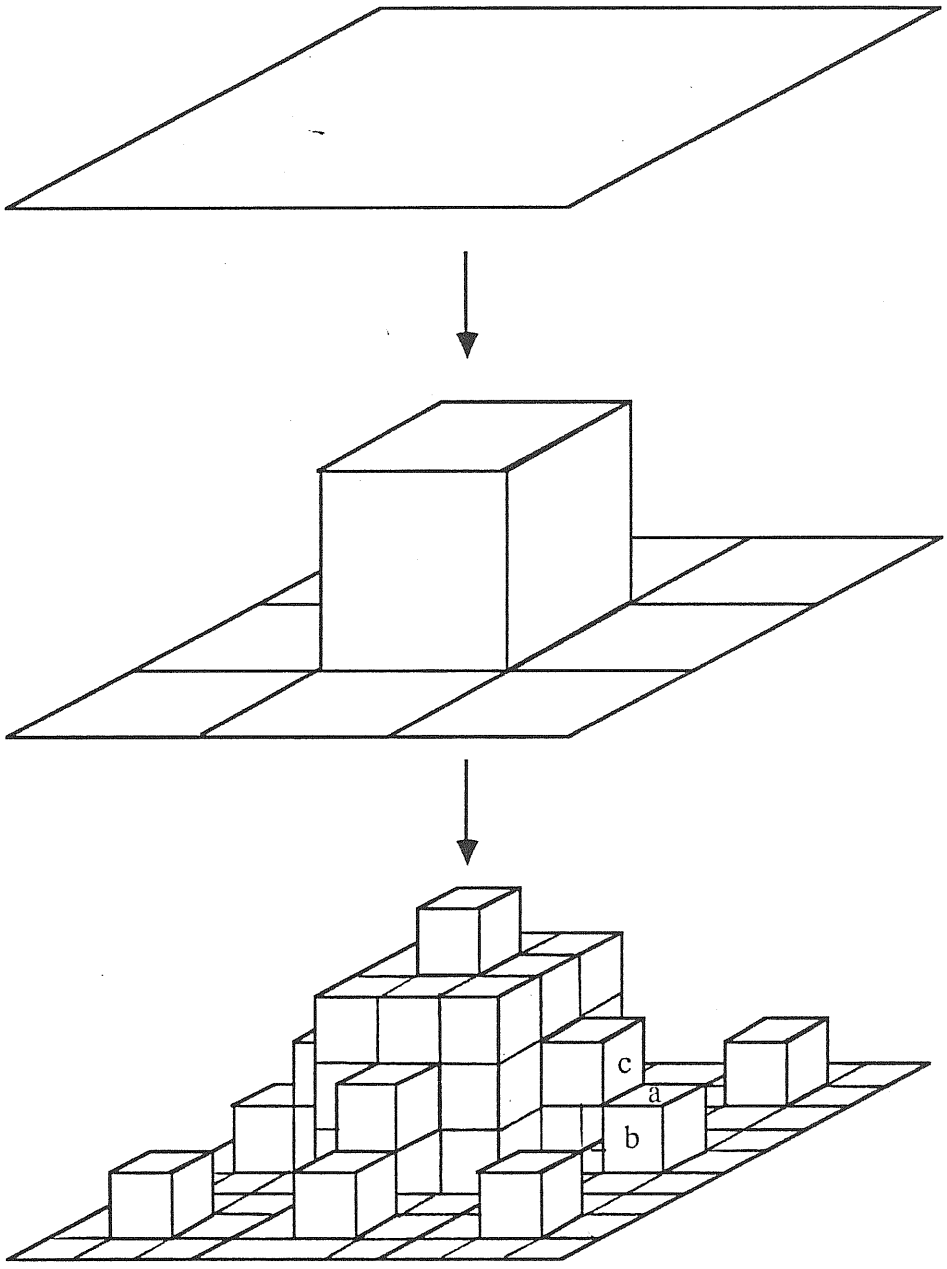

Fig. 5.1 The "hydrant" fractal surface. It is shown here its law of construction. In the lower part of the figure, the hydrant, when its construction law has been iterated for the second time is reported. In the calculation of the hydrant connectivity (see text) plaquettes a and b are connected while a and c plaquettes are not connected.

position of the walker will correspond to the coordinates of the center of the plaquette currently occupied.

The algorithm to perform the construction of the surface and to achieve the connectivity on of the surface according to wath we said above, was developed in such a way to avoid memory consumption. Using C-language we had the possibility to construct this algorithm in a recursive manner. The algorithm, moreover, allows to work with surfaces almost without limitations of extention, giving in principle the possibilty of making random walks of any length.

b) Performing random walks and calculating exponents

The algorithm mentioned above was used to generate the random walks on the fractal surface. A Monte Carlo procedure, was used to generate each walk. Both the end-to-end distance and the return probability functions were obtained by averaging over a large number of walks. The end-to -end distance function was obtained as

$$\langle r^2(n) \rangle = \frac{1}{N_W} \sum_{i=1}^{N_w} (\mathbf{r}_i(n) - \mathbf{r}_i(0))^2 \qquad (5.1)$$

where n is the step-index to be considered as the time t, while i individuates the i-th walk and N_W is the total number of walks. $(\mathbf{r}_i(n) - \mathbf{r}_i(0))^2$ represents the squared distance between the nth point and the corresponding starting point of the ith walk. In our procedure also the starting point was chosen at random on the surface.

$P_0(n)$ was estimated by collecting for each walk the return of its origine events. The average $P_0(n)$ was then obtained as

$$\langle P_0(n) \rangle = \frac{N_R(n)}{N_W} \qquad (5.2)$$

where $N_R(n)$ is the total number of return events occurred at the nth step for all the N_W walks.

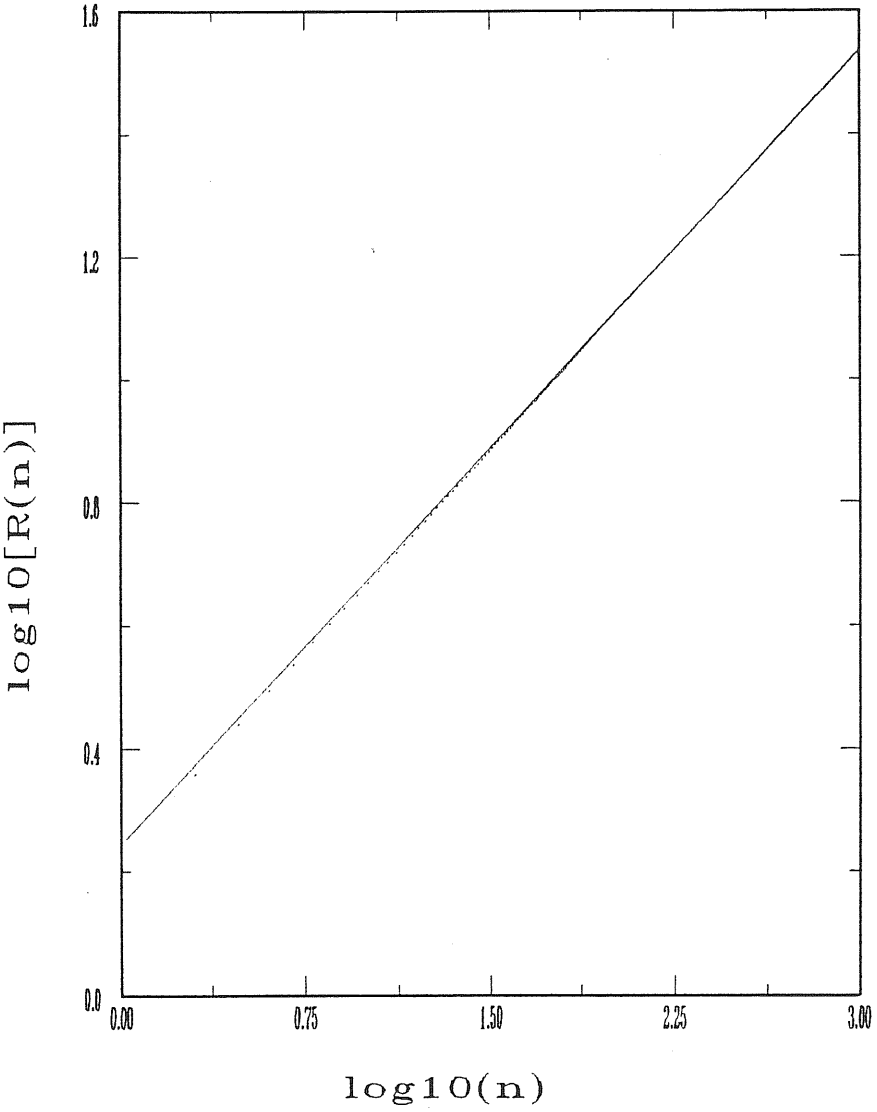

Fig. 4.7. Log-log plot of the $<r^2(n)>^{1/2}$ versus n for the hydrant fractal surface. In the calculation were considered walks 1000 steps long. The average was taken over 100000 walks. The slope of the streigth line drawn in the Fig. is m=.4296±.0002.

c) Results and discussion

Figs. 5.2 and 5.3 show the results for the $\langle r^2(n)\rangle$ and the $\langle P_0(n)\rangle$ obtained by the above mentioned Monte Carlo procedure. The diagrams display a well defined asymptotic behavior for the two quantities that allowed us to calculate the values of the exponents reported in the legends. From the expected form of $\langle r^2(n)\rangle$ and $\langle P_0(n)\rangle$ (i.e. $r \sim n^{1/d_W}$, and $P_0 \sim n^{-\tilde{d}/2}$, see also chapter 2) we could calculate the following values of d_W and $\tilde{d}$: $d_W = 2.3320 \pm 0.001$ and $\tilde{d} = 2.006 \pm 0.012$.

The values obtained for these two parameters are consistent with each other, as can be seen by using of the Alexander-Orbach relation ($\tilde{d} = 2\bar{d}/d_W$)[10]. Moreover we see that the estimated value of $\tilde{d}$, strongly suggest that the hydrant has a spectral dimensionality exactly equal 2.

Cates,[11] recently stated that the presence of a hierarchy of buildings in a random surface is expected to lead to a value of $\tilde{d}$ lower than 2. Our finding is in contrast with this claim. In this respect, the result we obtain, support the idea that the presence of buildings, even if disposed in a self-similar manner, is not sufficent to give anomalous spectral properties to a fractal surface. Some extra connectivity has probably to be assumed in order to change this result.

A further consequence of the above result $\tilde{d} = 2$ can be obtained with reference to the existing link between linear dynamics on a network, and conformational statistics of a "tethered surface" with the same network of connectivity.[12] It can be shown that $\tilde{d} = 2$ implies, for the "tethered surfaces" with hierarchical connectivity, the same ν (or $\bar{d}$) exponent, as far a surface with regular, two-dimensional connectivity.

Another direct application of the model discussed above can be the diffusion of, e.g., a molecular species (substrate) on a highly irregular, fractal boundary of a bigger molecular species (e.g. enzyme). What we find is that $d_W = \bar{d}$ in this case. So as

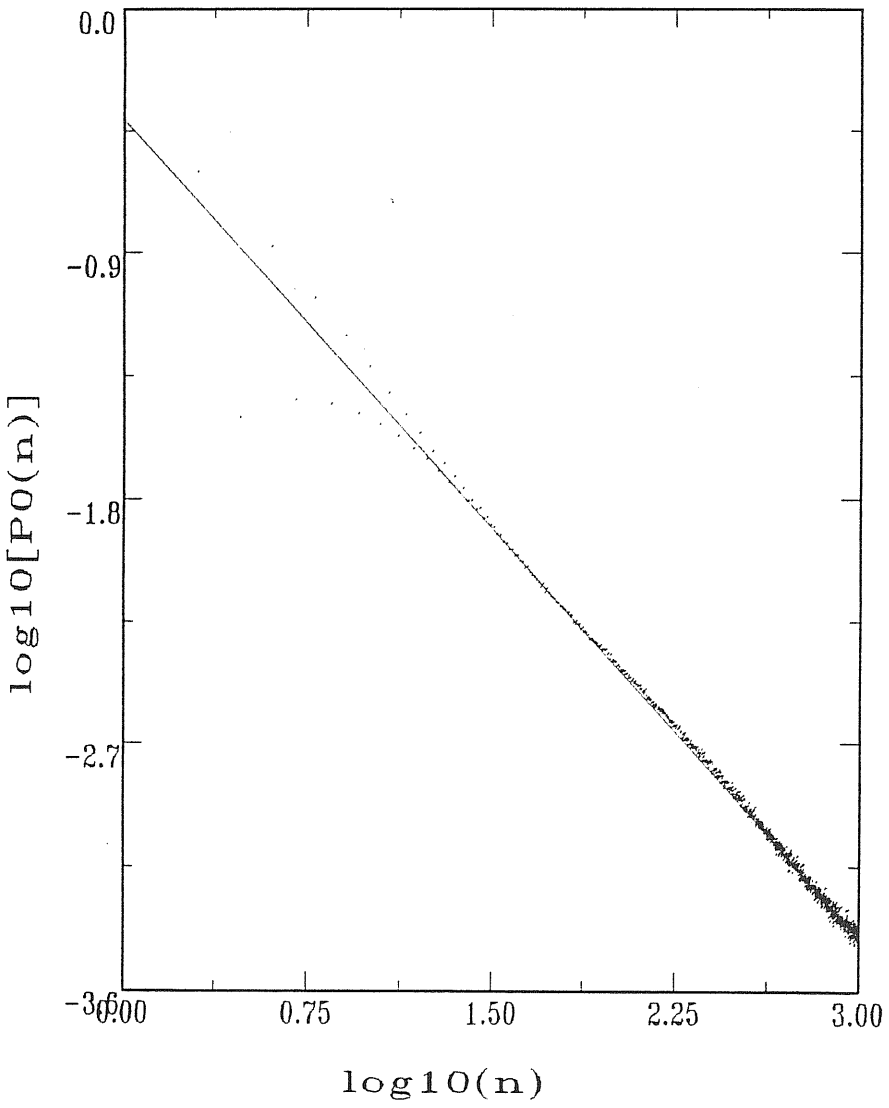

Fig. 4.8. Log-log plot of the $<P_0(n)>$ versus n for the hydrant fractal surface. In the calculation were considered walks 1000 steps long. The average was taken over 1000000 walks. The slope of the streigth line drawn in the Fig, is m= 1.003±0.006.

intuitive, the bigger $\bar{d}$, the slower the diffusion.

An extension of these calculations is under way. We are starting to consider the case of diffusion which does not take place exclusively on the surface, but is also allowed to visit one of the two subspaces bounded by the fractal surface. This kind of diffusion gives, e.g., information on the trapping probability by the fractal, for a molecule which diffuses in its neighborhood.

References

1. P.Pfeifer, U.Welz & H.Wipperman, *Chem.Phys.Lett.*, **113**, 535(1985)
2. D.Avnir, D.Farin & P.Pfeifer, *NATURE*, **308**, 261(1984)
3. G.Parisi, *Phys.Lett.*, **B 81**, 357(1979)
4. D.J.Gross, *Phys.Lett.*, **B 138**, 185(1984)
5. J.B.Kogut, *Rev.Mod.Phys.*, **55**, 755(1983)
6. J.M.Drouffe, G.Parisi & N.Sourlas, *Nucl.Phys.*, **B 161**, 397(1983)
7. A.Maritan & A.Stella, *Phys.Rev.Lett.*, **53**, 123(1984)
8. U.Glaus, *Phys Rev. Lett.*, **56**, 1996(1986)
9. M.Karowsky, *J.Phys.*, **A 19**, 3375(1986)
10. S.Alexander & R.Orbach, *J.Phys.Lett.***43**,L625(1982)
11. M.E.Cates, *Phys.Lett.*, **161 B**, 363(1985)
12. A.Maritan & A.Stella, *Phys. Rev. Lett.*, **59**, 300(1987)

Acknowledgements

I would like to thanks Prof. Harvey Stapleton and his collaborators for the hospitality and the assistance, during my permanence in their lab. Thanks are also due to Dr. Franca Aicardi for her invaluable help in the developing of the computer algorithm for construction of the fractal surface. I also acknowledge Prof. Attilio Stella for his help in the course of all thesis.